Icarus 318 (2019) 147–169

Contents lists available at ScienceDirect

Icarus

journal homepage: www.elsevier.com/locate/icarus

Mineralogy mapping of the Ac-H-5 Fejokoo quadrangle of Ceres

S. Singh[a], J-P. Combe[a], L.A. McFadden[b,*], T.B. McCord[a], K.H.G. Hughson[d], F. Zambon[c], M. Ciarniello[c], F.G. Carrozzo[c], A. Raponi[c], E. Ammannito[d], M.C. De Sanctis[c], A. Frigeri[c], O. Ruesch[b], F. Tosi[c], A. Longobardo[c], E. Palomba[c], C.A. Raymond[e], C.T. Russell[d]

[a] Bearfight Institute, 22 Fiddler's Road, P.O. Box 667, Winthrop, WA 98862, USA
[b] NASA Goddard Space Flight Center, Greenbelt, MD, USA
[c] INAF-IAPS Istituto di Astrofisica e Planetologia Spaziali, Rome, Italy
[d] IGPP, University of California at Los Angeles, Los Angeles, CA, USA
[e] Jet Propulsion Lab, Pasadena, CA, USA

ARTICLE INFO

Keywords:
Dwarf planet
Asteroids
Surface composition
Spectroscopy

ABSTRACT

This paper focuses on the identification and distribution of compositional units and their stratigraphic relationships in the Fejokoo quadrangle of Ceres (Ac-5) located between 21–66°N and 270–360°E and named after one of its prominent and well-preserved impact craters, Fejokoo (centered at 26°N and 312°E). In this quadrangle, we observed that hydroxylated- (OH-rich) and ammoniated- (NH_4-rich) phyllosilicates are present everywhere, in various abundances; low abundance is observed on bright terrains and higher abundances are observed on lobate materials associated with craters. Carbonates are mostly correlated with the high-albedo areas surrounding Oxo (359.7°E, 42.2°N) and other major craters, and are mixed with Ceres' most common surface composition type (i.e. low albedo, phyllosilicate-rich material). There are a few locations where carbonates and phyllosilicates co-exist, indicating a range of geological or chemical processes produced them in co-existence. No correlation between the surface composition and the age of the craters was found. Instead, the composition observed on impact craters depends on the size of the impact and the composition of the different stratigraphic layers excavated. The compositional interpretation inferred from Dawn's visible-infrared spectrometer data of the Fejokoo quadrangle is consistent with the presence of an internal ocean that produced carbonates and phyllosilicates via aqueous alteration of minerals.

1. Introduction

Since the early 1970s, Ceres has been studied extensively by telescopic observations from the ground and in orbit around the Earth. The Dawn spacecraft began orbiting Ceres in March 2015 (Russell et al., 2016). It subsequently acquired remote-sensing data with the Framing Camera (FC, Sierks et al., 2011), the Visible and InfraRed mapping spectrometer (VIR, De Sanctis et al., 2011) and the Gamma-Ray and Neutron Detector (GRaND, Prettyman et al., 2011) for geological and compositional mapping. In addition, monitoring of its position and attitude by means of radio science provided data for gravity and geophysical models and placed constraints on Ceres' interior structure (Konopliv et al., 2011; Park et al., 2016). Ceres is the largest object (473 km mean radius) and the most massive in the main asteroid belt. It is large enough to have experienced many of the processes normally associated with planetary evolution, such as differentiation (McCord and Sotin, 2005), and has since been classified as a dwarf planet (International Astronomical Union, 2006, https://www.iau.org/news/pressreleases/detail/iau0603/accessed 1/11/2018). Ceres' relevance to the terrestrial planets and icy bodies like Europa makes it an ideal candidate for exploring the early stages of planetary formation and gaining insight into planetary evolution.

The Dawn mission has shown that Ceres is an active body with substantial amounts of water present beneath its surface (Prettyman et al., 2017). Prior to Dawn's arrival at Ceres, bright surface materials were initially interpreted as salts that formed in the early stages of Ceres' history (McCord and Sotin 2005; Castillo-Rogez and McCord, 2010). During the differentiation of Ceres, contact between silicates and ice or liquid water resulted in aqueous alteration of minerals, producing hydroxylated (OH-bearing) phases such as phyllosilicates, carbonates, or mineral hydrates (King et al., 1992; Rivkin et al., 2006; Milliken and Rivkin, 2009). Analysis of VIR spectra later suggested that these bright areas of high albedo are consistent with large amounts of sodium carbonates (De Sanctis et al., 2016), implying that

* Corresponding author.
E-mail address: lucy.mcfadden@nasa.gov (L.A. McFadden).

https://doi.org/10.1016/j.icarus.2018.08.025
Received 10 May 2017; Received in revised form 28 August 2018; Accepted 28 August 2018
Available online 30 August 2018
0019-1035/

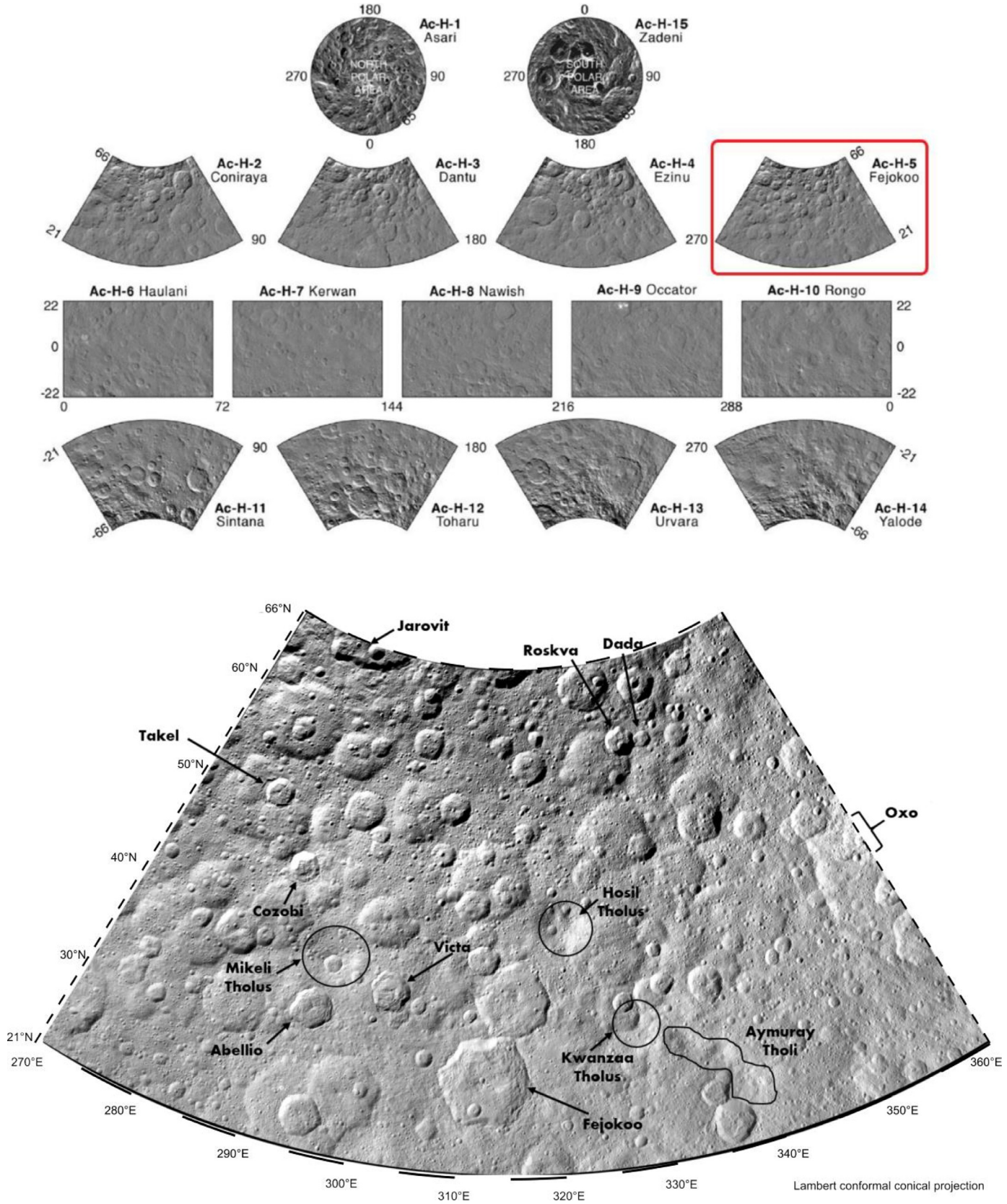

Fig. 1. Regional maps of the entire surface of Ceres organized in a 15-quadrangle scheme. Top: figure is adapted from Roatsch et al. (2016). The Fejokoo quadrangle (framed), is located at 270°–360°E, 21°–66° N. Bottom: Dawn FC clear filter Low Altitude Mapping Orbit (LAMO) base map mosaic in the Lambert Conical projection, with 35 m/pixel resolution, (Roatsch et al., 2017).

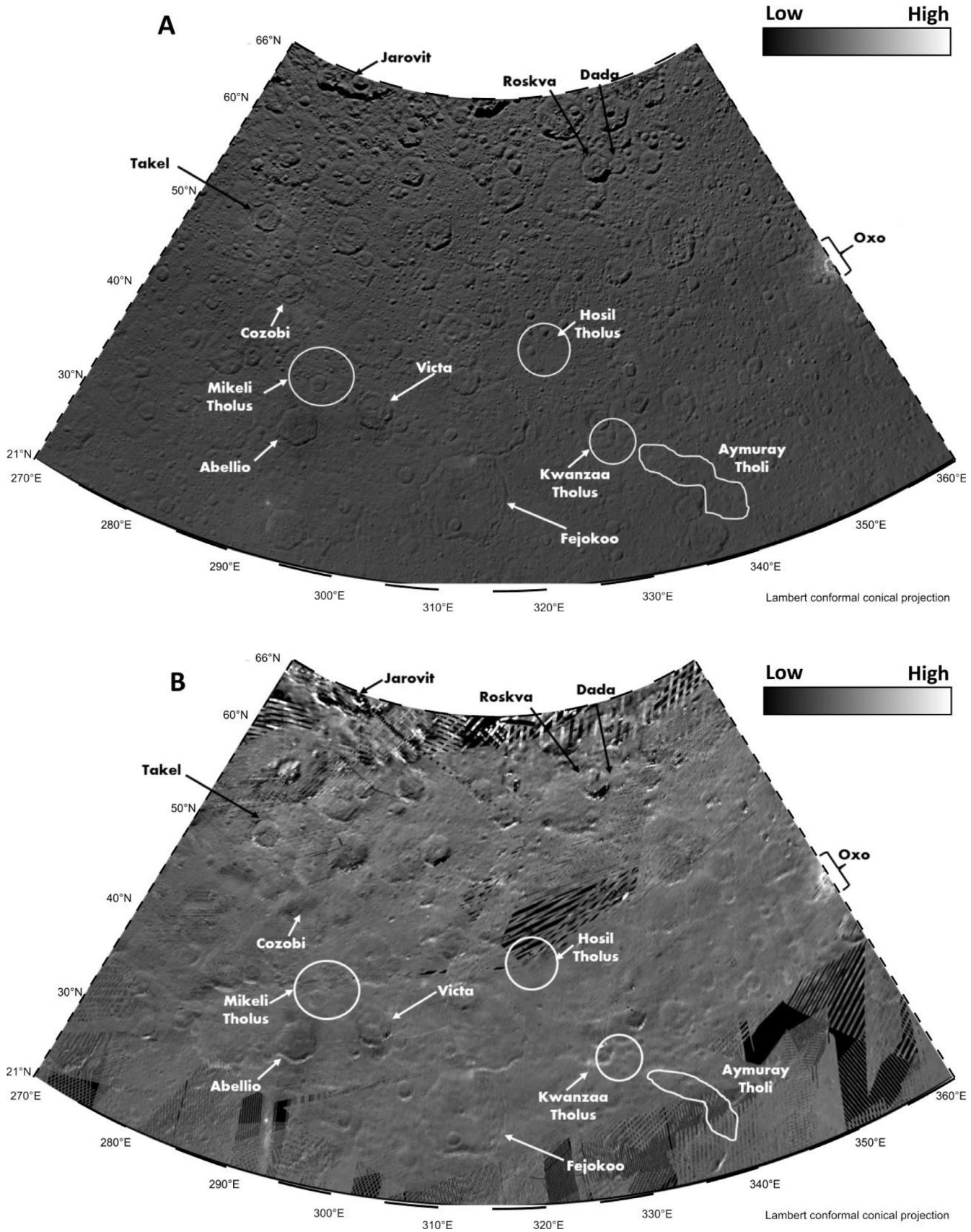

Fig. 2. Maps of the Fejokoo quadrangle: (A) Photometrically corrected FC albedo map at 0.75 μm, (B) Albedo map from VIR at 1.2 μm.

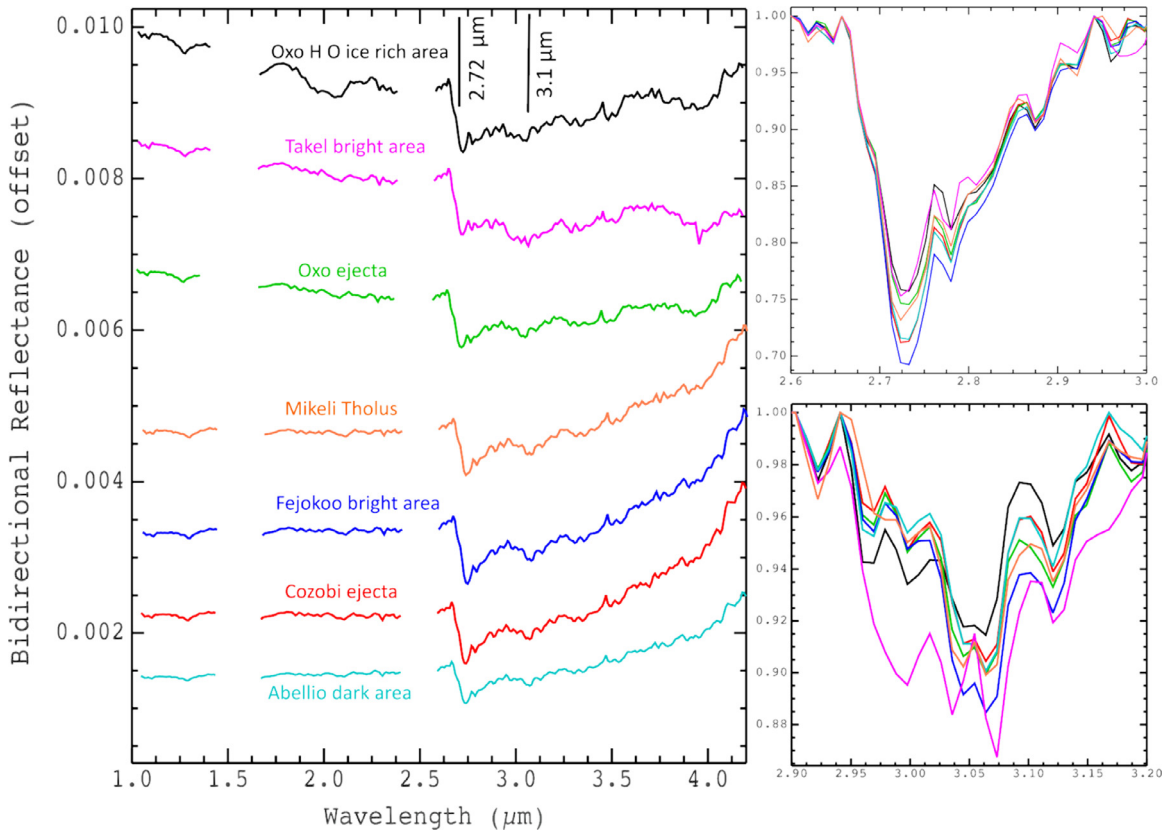

Fig. 3. Spectral profiles of the major geological units in the Fejokoo quadrangle from 1.0–4.2 µm, no thermal correction applied. Gaps in wavelength coverate indicate regions corresponding to boundaries between diffraction gratings in VIR (DeSanctis et al., 2011).

recent geologic activity was involved in their formation, consistent with evidence of also recent aqueous alteration of silicates (Ammannito et al., 2016).

Ceres' average geometric albedo is 0.11 (Li et al. 2015), and the global average spectrum has absorption bands attributable to mixtures of Mg, Fe, and NH_4- (ammoniated) phyllosilicates (De Sanctis et al., 2015; Ammannito et al., 2016). The spectral signature of Na-carbonates is also present across the surface (Milliken and Rivkin, 2009; De Sanctis et al., 2016), and H_2O absorption bands are absent at global scales (De Sanctis et al., 2015), but present on a few small areas (Combe et al., 2016, 2017, Raponi et al., 2018).

The objective of this study is to analyze reflectance spectra of surface features in the Fejokoo quadrangle (Ac-5) located within 21–66°N and 270–360°E, and interpret the distribution of surface components (Fig. 1). Our strategy is to address the following:

(1) Identify the surface components in this quadrangle and determine their distribution.
(2) Compare the surface composition in this quadrangle with the global interpretation of Ceres' surface and other quadrangle studies (see McCord and Zambon, 2018).
(3) Determine whether any correlations exist between morphological features and surface composition.
(4) Find implications of the compositional maps in context with the geology for the formation and evolution of Ceres.

Hughson et al. (2017) describe the terrain in Fejokoo as highly cratered, and Jaumann et al. (2016) determine the region to be among the oldest on Ceres. The largest crater in this region, Fejokoo, has a hexagonal rim. Topography (Preusker et al., 2016) - reveals six tholi (domical mountains) in this quad (Hughson et al. 2017). Although the topography is marked and morphological features are diverse, the spectral reflectance is largely uniform, as indicated by the maps of several of the most significant spectral parameters sensitive to absorption bands. Dawn has detected H_2O absorption features within a low-illumination, highly reflective zone in Oxo (359.7°E, 42.2°N) (Combe et al., 2016), a 10-km diameter, geologically fresh crater. The presence of H_2O ice in Oxo is consistent with a generally H_2O-rich subsurface as seen by GRaND (Prettyman et al., 2017), lobate flows and fractures that show landslides driven by H_2O ice may have occurred, and a terrace on the southeastern side which appear as the rim and wall have collapsed towards the center of the crater. Laboratory experiments (Clark, 1984; McCord et al., 2002; Hanley et al., 2014) indicate that the spectra of hydrated minerals have H_2O absorption bands that are distorted and shifted with respect to those of pure H_2O, which are clearly distinct from H_2O ice adsorptions seen at Oxo. Oxo falls within the limits of the Fejokoo quadrangle, and thus a closer look at Oxo mineralogy is one objective of this study.

In order to map the surface composition of Ceres' quadrangles, several mapping products calculated from VIR data are used together (Frigeri et al., 2018), including albedo maps and absorption band depths at 2.72 and 3.1 µm, respectively due to OH- (hydroxyl) and NH_4- (ammonium) bearing minerals. We also calculated specific spectral parameters from VIR data, such as absorption bands at 3.43 and 4 µm, to study the composition of carbonates, as well as two-parameter color composites and three-color composites to aid in synthesized analyses. In addition, we used a high-resolution atlas of Ceres at a scale of 1:750,000 (Fig. 1, bottom) derived from ~2490 clear images acquired with Dawn spacecraft's Framing Camera (Roatsch et al., 2016) with pixel resolution of 140 m/pixel, altitude of 1475 km, and photometrically-corrected albedo maps Schröder et al., 2017).

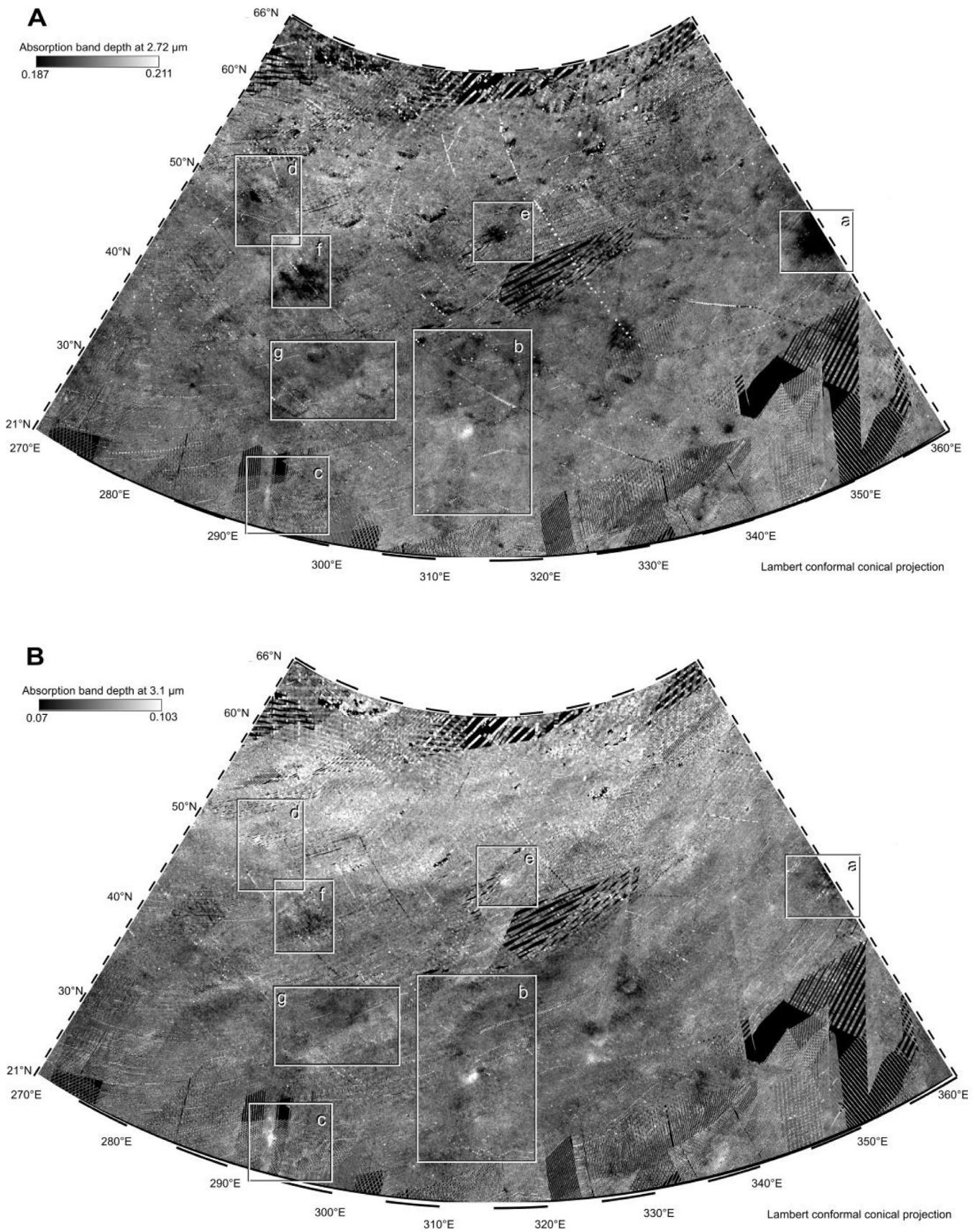

Fig. 4. Maps of the Fejokoo quadrangle showing the absorption band depth at 2.72 μm (A) and at 3.1 μm (B) from VIR observations. The rectangles correspond to close-up views of areas of interest: (a) Oxo crater, (b) Fejokoo and Sedana craters, (c) Kaneki crater and surrounding region, (d) Takel crater, (e) Jumi crater, (f) Cozobi crater and (g) Abellio and Victa craters.

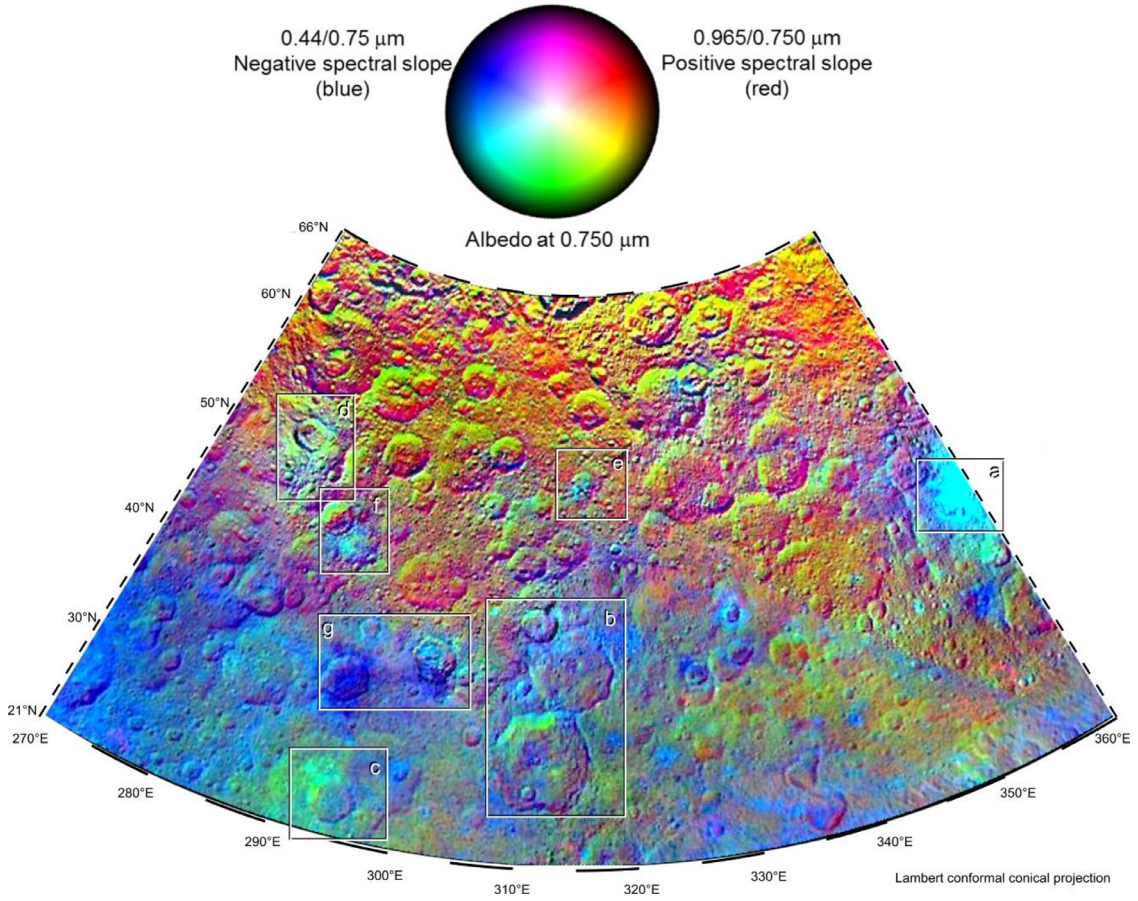

Fig. 5. Map of the Fejokoo quadrangle showing a color composite map obtained from FC data using the following color combination: Red: positive spectral slope at 0.965 μm /0.75 μm, Blue: negative spectral slope at 0.44 μm/0.75 μm, Green: geometric albedo at 0.75 μm. The rectangles correspond to close-up views of areas of interest: (a) Oxo crater, (b) Fejokoo and Sedana craters, (c) Kaneki crater and surrounding region, (d) Takel crater, (e) Jumi crater, (f) Cozobi crater and (g) Abellio and Victa craters.

2. Data sets and methodology

2.1. Dawn's optical instruments

2.1.1. The Framing Camera (FC)

Framing Camera (Sierks et al., 2011) images with a field of view (FOV) of 5° × 5°, and an instantaneous field of view (IFOV) of 93.7 μrad/pixel were acquired with a resolution of 62 m per pixel at Ceres. Mosaics were produced to provide geological and geomorphological context using one clear filter and seven color filters with bandpasses centered between 0.4 and 1.0 μm. The FC system provides both high signal to noise ratio and high spatial resolution. Several maps in this study rely on the photometrically-corrected (normal albedo) clear filter, global map (Schröder et al., 2017) and a color composite in order to analyze the spectral and geological properties of Ceres. This step is essential to study the stratigraphy and the relationship between the compositional units both globally and regionally, within the Fejokoo quadrangle.

2.1.2. The Visible and InfraRed mapping spectrometer (VIR)

VIR (De Sanctis et al., 2011) is an imaging spectrometer with an IFOV of 250 × 250 μrad and FOV of 64 × 64 mrad. It has two detectors: one sensitive to visible radiation in the range 0.25–1.05 μm, and an infrared detector in the range 1.0–5.0 μm, with a spectral sampling of 1.8 nm and 9.8 nm, respectively. Depending on the altitude of the spacecraft the nominal pixel resolution varies for the Survey (0.676 and 0.719 km/pixel), High Altitude Mapping Orbit (HAMO, 0.161 and 0.206 km/pixel), and Low Altitude Mapping Orbit (LAMO, 0.043 and 0.075 km/pixel). Artifacts have been removed according to the processes reported by Carrozzo et al. 2016. The reflectance spectra of minerals contain absorption features that are diagnostic of mineralogy, grain size, and crystal structure. In this paper, we used VIR spectral parameter maps sampled at 140 m/pixel data by Frigeri et al., 2018. They are mosaics of multiple observations acquired from Dawn's Survey and HAMO mission phases. For local analyses of carbonate distribution, we also used VIR spectra from LAMO.

2.2. Albedo maps

Albedo maps are images of the surface that are corrected for photometric effects due to topography, the physical characteristics of the regolith, and the geometry of illumination and observation (the incidence, emergence and phase angles). Photometric correction of the FC data is reported by Schröder et al. (2017). In Fig. 2A, we show the photometrically corrected map of the Fejokoo quadrangle obtained from HAMO (Ac-H-5). Towards the northern portion of the quadrangle, there are photometric residuals (e.g. apparent crater rims) due to both topography and high incidence angle that cast shadows where the signal is too low for the model to make corrections. If the photometric correction were perfect, crater rims would not stand out. It is important to account for such artifacts when interpreting the surface composition using albedo maps. High-albedo areas such as Oxo's ejecta, a small area on Fejokoo crater's northern wall, and others are easily identified. Two craters named Abellio and Victa and their ejecta show a lower albedo than the surrounding terrain. Fig. 2B shows the photometrically corrected reflectance at 1.2 μm obtained from VIR, derived from Hapke

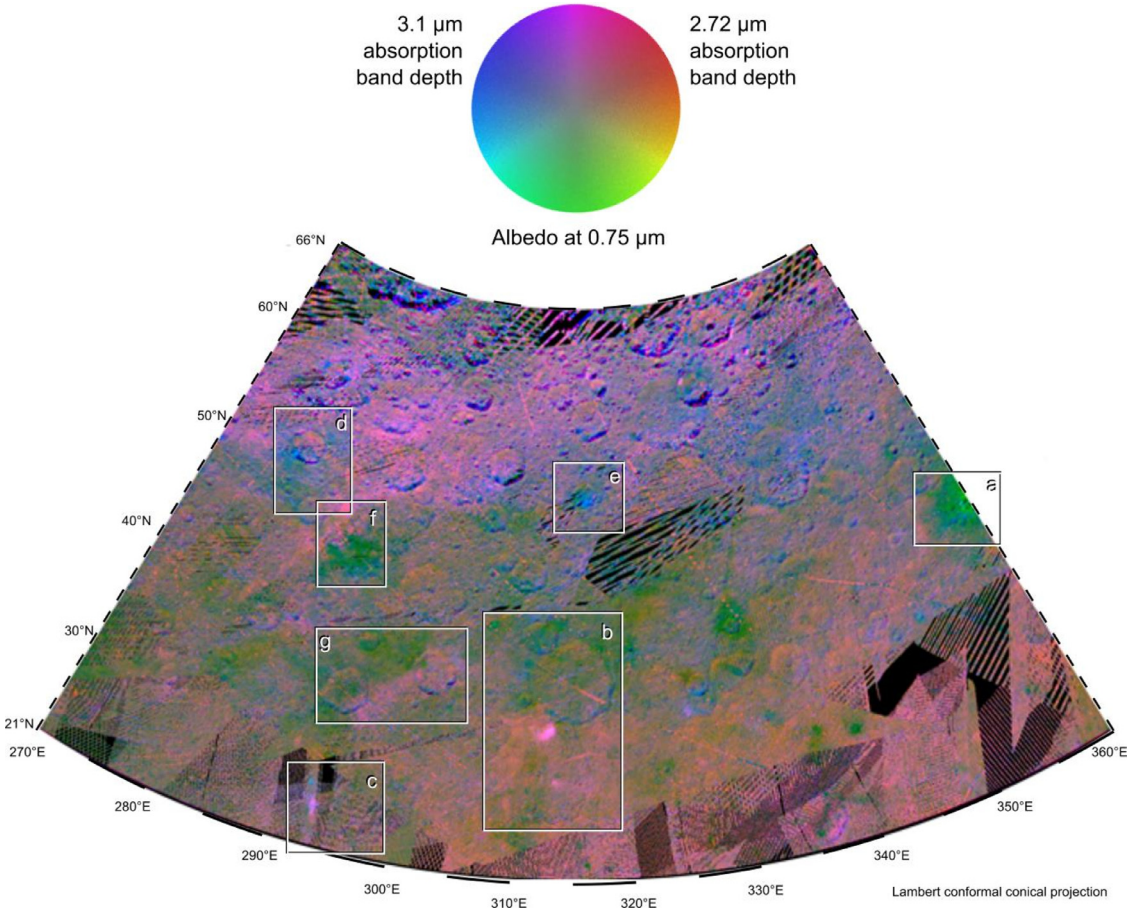

Fig. 6. Map of the Fejokoo quadrangle showing a color composite map obtained from FC and VIR data using te following color combination: R = BD at 2.72 μm, G = FC albedo at 0.45 μm, B = BD at 3.1 μm. The rectangles correspond to close-up views of areas of interest: (a) Oxo crater, (b) Fejokoo and Sedana craters, (c) Kaneki crater and surrounding region, (d) Takel crater, (e) Jumi crater, (f) Cozobi crater and (g) Abellio and Victa craters.

modeling (Hapke, 1981) of the average surface photometric properties of the body (Ciarniello et al., 2017; De Sanctis et al., 2016).

2.3. VIR absorption band parameters and maps

Absorption band depths were calculated at 2.72 and 3.1 μm where Ceres' surface spectra are dominated by absorption bands centered at these wavelengths (Fig. 3), indicating the widespread occurrence of OH- and NH_4-bearing phyllosilicates (Ammannito et al., 2016). Prior to the Dawn mission, the absorption band at 3.1 μm had been attributed to a variety of different phases including water ice, hydrated or NH_4 -bearing clays and brucite (Lebofsky et al. 1981, Feierberg et al., 1981; King et al., 1992; Rivkin et al., 2006; Milliken and Rivkin, 2009; De Sanctis et al., 2015). With Dawn, spectral modeling of VIR data (De Sanctis et al., 2015; Ammannito et al., 2016) has related the 3.1 μm absorption band to ammoniated phyllosilicates, such as NH_4-bearing annite, antigorite, and NH_4-montmorillonite. The strong and narrow absorption centered at 2.72 μm is a characteristic feature of OH-bearing minerals (Clark, 1999; Carry et al., 2008; De Sanctis et al., 2015). The ubiquitous presence of absorption bands at 2.72 and 3.1 μm is characteristic of widespread distribution of phyllosilicates and ammonium-bearing phyllosilicates, respectively (De Sanctis et al., 2015), with lateral variations in abundance but not in chemistry (Ammannito et al., 2016). Fig. 3 shows VIR spectra of the primary geological features in the Fejokoo quadrangle.

The spectral band parameter maps were derived using methods described in Frigeri et al. (2018). Absorption band depth is calculated by measuring the distance between the deepest part of the band and a straight-line continuum between two fixed wavelengths on either side of the absorption band. The quadrangle maps of absorption band depth at 2.72 μm and 3.1 μm are shown in Fig. 4A and B, respectively. Strong band depths correspond to the Fejokoo crater's bright material on its south-facing wall and a few areas of bright material near Cozobi crater. We observe weak band depths that correspond to Oxo crater and its ejecta in the north-west direction; and also near Cozobi crater's southern lobate flow. Other areas with both weak 2.72 μm and 3.1 μm absorption bands are discussed in Section 3. In the Fejokoo quadrangle, the extremely low values of the 2.72 μm and 3.1 μm absorption bands correspond to Oxo crater, indicating low abundance of both OH- and NH_4-bearing phyllosilicates. Absorption band depths do not show any positive correlation with albedo or reflectance values.

2.4. Three-color composites

2.4.1. Visible albedo and spectral slope

Fig. 5 is a color composite map of band ratios where red represents positive spectral slope at 0.965 μm /0.75 μm, blue the negative spectral slope at 0.44 μm/0.75 μm, and green is geometric albedo at 0.75 μm using the color ratios used by Pieters and Tompkins (1999) for the Earth's moon. Light blue color typically represents high albedo with negative spectral slope, dark blue indicates low albedo with a negative spectral slope, and yellow indicates high albedo with slightly positive spectral slope. These displayed color differences would appear fairly uniform to the human eye in natural color. Enhancing them provides valuable insights into the mineral composition of the surface, as well as the relative ages of surface features. The negative slope with bright

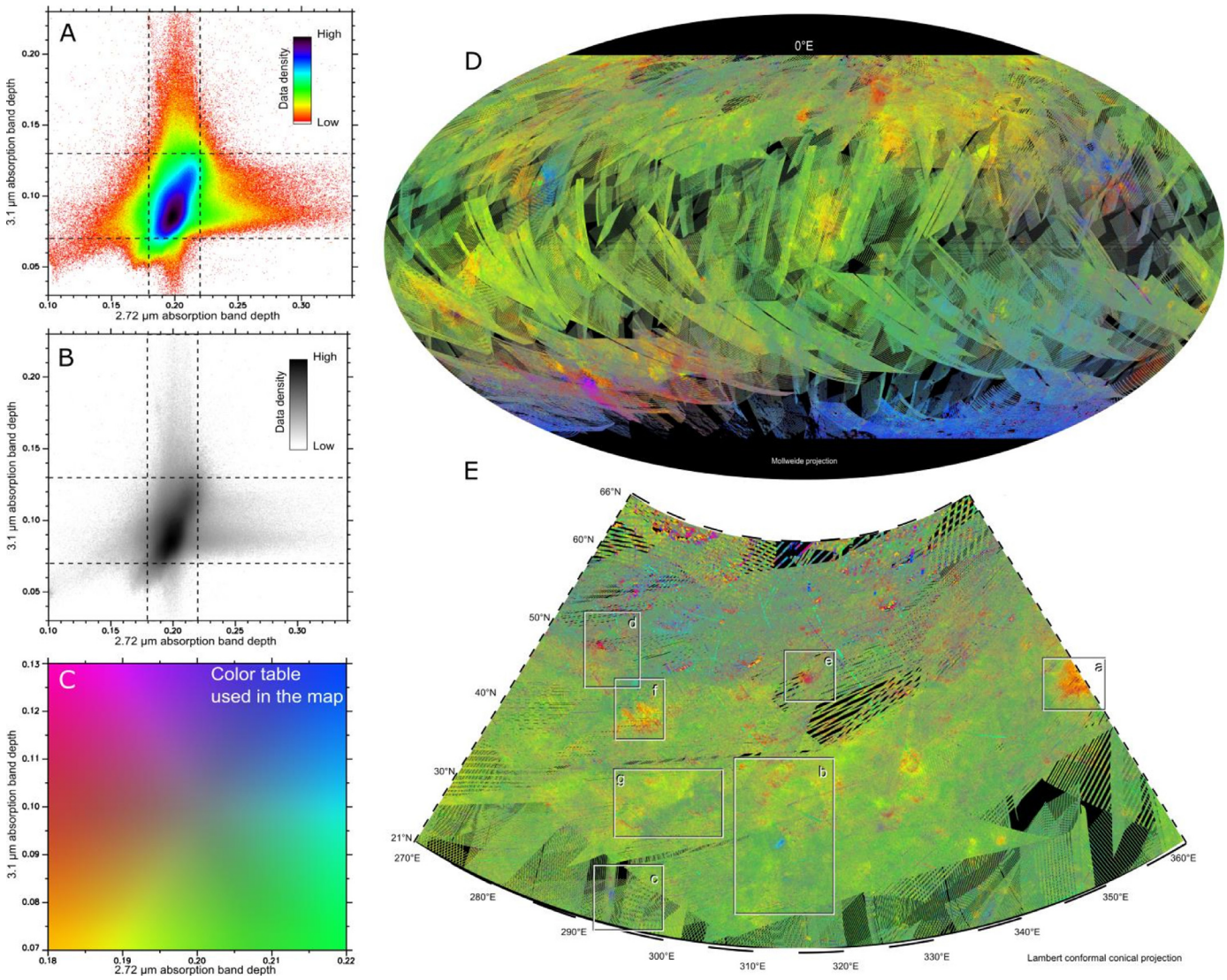

Fig. 7. Mapping and analysis of absorption bands at 2.72 µm and 3.1 µm at the surface of Ceres. (A-B panels): a 2D scatter plot of the total surface of Ceres observed by VIR for the absorption band depth at 3.1 µm as a function of 2.72 µm absorption band depth. (C)The 2D color scale define the colors represented in the global map of Ceres and the regional map of the Fejokoo quadrangle. (D) The global map is projected in Mollewide projection. (E) The regional Fejokoo quadrangle map is projected in Lambert Conical projection. The rectangles correspond to close-up views of areas of interest: (a) Oxo crater, (b) Fejokoo and Sedana craters, (c) Kaneki crater and surrounding region, (d) Takel crater, (e) Jumi crater, (f) Cozobi crater and (g) Abellio and Victa craters.

areas represents relatively younger surface and material excavated from beneath the surface, whereas the positive spectral slope indicates darker surface.

2.4.2. *Visible albedo and absorption band depth*

Fig. 6 was produced by combining FC albedo map and VIR 2.72 µm and 3.1 µm absorption bands with the following color combination: red = 2.72 µm absorption band depth, green = FC albedo at 0.45 µm, blue = 3.1 µm absorption band depth. The albedo map used is affected by photometric effects at higher latitude due to low illumination and shadows because of high incidence angles. As a result, sharp color variations between blue and magenta near crater rims are artifacts that correspond to deep shadows and fully illuminated areas respectively. We don't offer mineralogical interpretation of these regions due to the predominance of artifacts.

2.4.3. *Two-parameter color composites*

In order to display the distribution of the 2.72 and 3.1 µm band depths in this quadrangle in the context of Ceres' global composition, we used the technique described in Combe et al. (2018). These maps show the overall distribution of the 2.72 and 3.1 µm absorption band depths using a two-dimension, multi- color scale. A two-dimensional scatter plot of the total surface of Ceres observed by VIR for reflectance at 2.72 µm as a function of the 3.1 µm absorption band depth is shown in Fig. 7A. Values are scattered over the entire range of the displayed graph; however, the highest density of points is concentrated near the center of the plot, represented in dark colors in Fig. 7A and B. On the other hand, there are outliers that correspond to extreme values of the absorption band depths that may happen if fresh and pure mineral components are exposed at the surface. However, these outliers can also be caused by instrument calibration residuals, photometric effects due to topography, and possibly effects of spatial sampling resulting from projections containing data gaps. We show maps in two different color schemes. In Fig. 7C, all the pixels are represented in color: this scheme is convenient for interpreting variations at global or regional scales. Regions in green indicate areas with relatively high abundance of OH phyllosilicates (strong absorption at 2.72 µm) and low abundance of NH_4 phyllosilicates (weak absorption at 3.1 µm). The region in blue indicates areas with relatively high 2.72 and 3.1 µm band depth, whereas yellowish color represents the low value of both 2.72 and

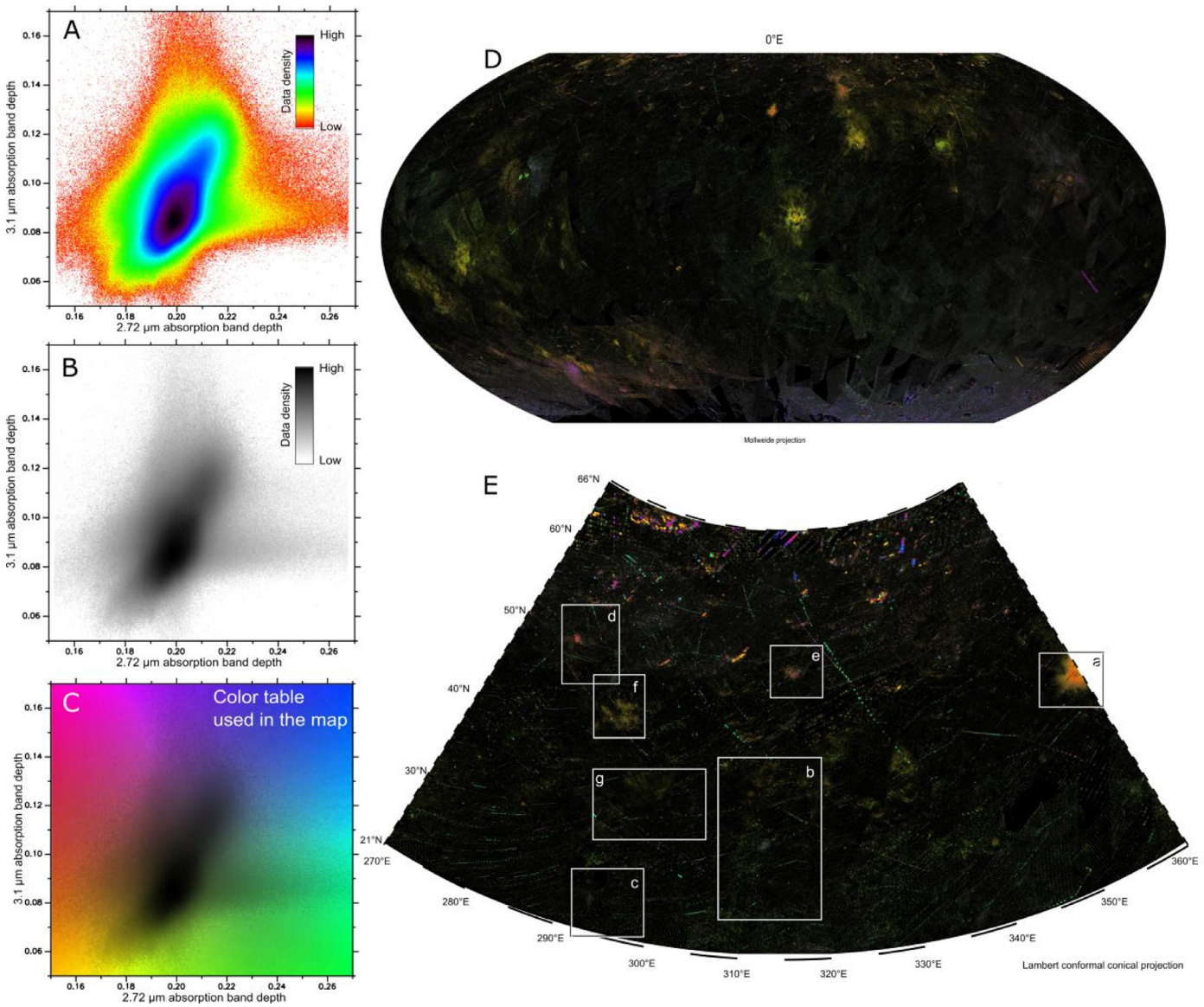

Fig. 8. Mapping and analysis of absorption bands at 2.72 μm and 3.1 μm at the surface of Ceres. A and B with a small change in scale, are the same as Fig. 7, except the 2D-scatter plot that overlays the color square panel (C) is used as a mask on the global map (D) of Ceres and on the regional map of Ac-H-05 quadrangle (E) which highlight the end-member (purest) compositions. The rectangles correspond to close-up views of areas of interest: (a) Oxo crater, (b) Fejokoo and Sedana craters, (c) Kaneki crater and surrounding region, (d) Takel crater, (e) Jumi crater, (f) Cozobi crater and (g) Abellio and Victa craters.

3.1 μm band depths. The cyan and yellow-orange region define a spatially-coherent region including Fejokoo crater, Cozobi crater, and Oxo's ejecta.

In Fig. 8, the pixels with the most common compositions displayed as green in Fig. 7, are displayed in black, with the global 2D density scatter plot overlain on the 2D color scale. The purpose is to enhance the pixels of areas with the most extreme compositions. In this representation, the majority of Ceres' surface appears black (average composition); only the extreme compositions such as Oxo, Haulani (Tosi et al., 2018), Ernutet (Raponi et al., 2017), and Occator (Longobardo et al., 2017) have colors, indicating that they are distinct from the global mineral surface composition. Oxo's composition is unique compared to rest of the quadrangle. Small compositional variations are enhanced in Cozobi, Fejokoo bright streaks, and Takel crater's bright spot (see Fig. 2 for location names).

To enhance the most extreme values of the spectral parameters on the maps, we adjusted the band depth ranges to better represent the data over the Fejokoo quadrangle (Fig. 9). A two-dimensional scatter plot of the 2.72 μm absorption band as a function of the 3.1 μm absorption band for the area covered by the Fejokoo quadrangle is shown in Fig. 9A. In addition, the data density cloud of quadrangle Fejokoo is overlain on the color scheme of Fig. 9B to create the color table (Fig. 9C) used in the map (Fig. 9D). The colors appear to be related to geological features, such as crater ejecta, flows, or bright materials. Oxo is the brightest and most spectrally distinct feature in the quadrangle, however, the regional variation in phyllosilicate band values is also apparent. The 2.72 μm absorption band is fairly uniform throughout the quadrangle; however, the variation in 3.1 μm absorption band depth is large at areas such as Takel and the bright material of the crater Jumis (51.6°N, 316.4°E). There are several areas where both absorption bands at 2.72 μm and 3.1 μm are weak, such as Cozobi's lobate material, and stronger at other locations, such as Fejokoo's bright material. The localized compositions of each extreme region are discussed below in Section 3. Maps in Fig. 10 are the 2.72 and 3.1 μm band depth maps overlaid on the FC clear-filter map. These maps help to show the topography and facilitate the location of extreme composition with respect to impact craters. Fig. 10A corresponds to Fig. 7E and Fig. 10B corresponds to Fig. 9D.

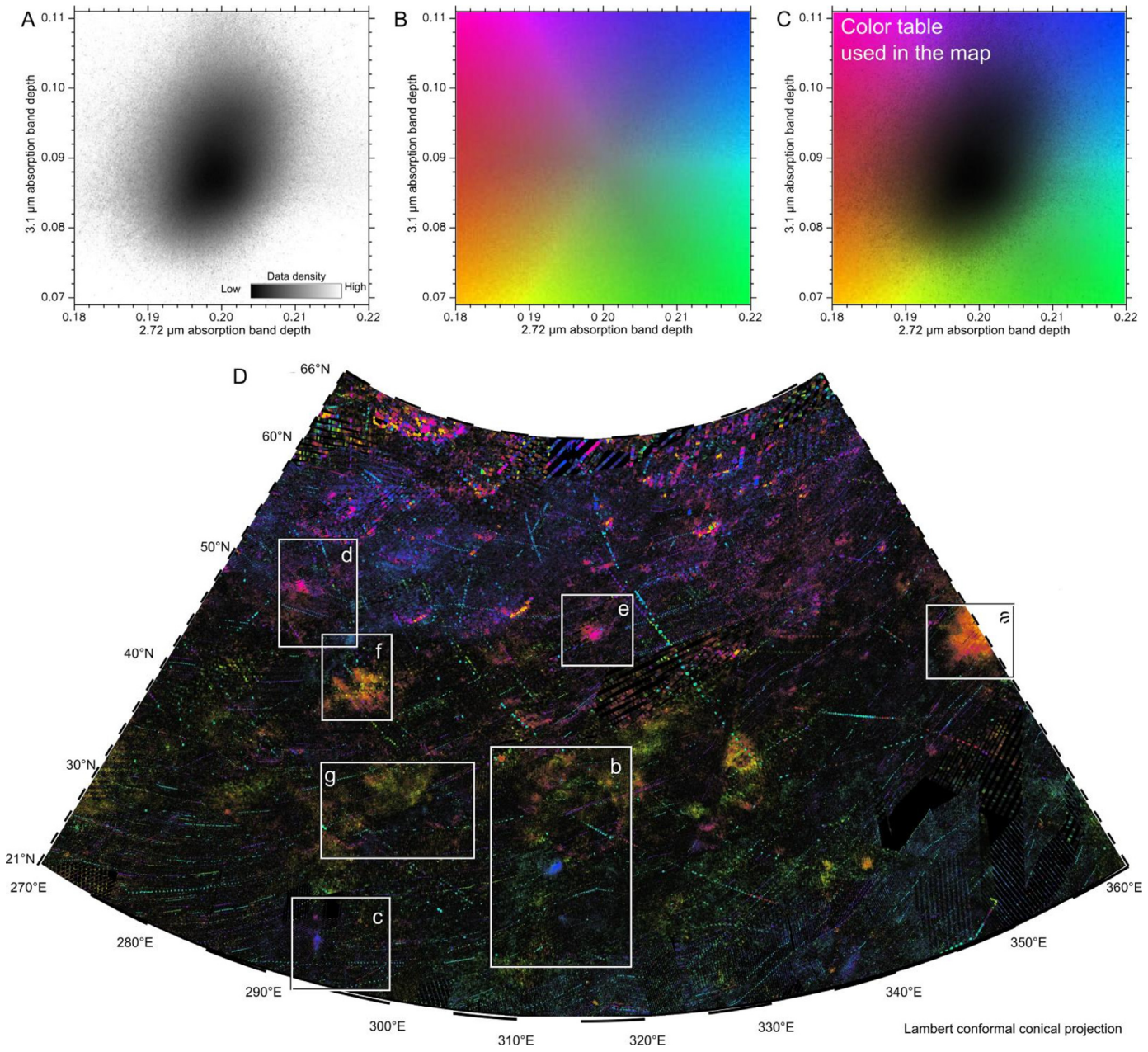

Fig. 9. Mapping and analysis of absorption bands at 2.72 μm and 3.1 μm at the surface of Ceres. (A) The two-dimensional scatter plot corresponds to the 2.72 μm as a function of 3.1 μm absorption band depth over the surface of the Fejokoo quadrangle. (B) The colored square is the background for panel C. (C) The color table combines the colored square (B) overlain by the 2D-scatter plot (A), using the same technique as Fig. 8C. (D) Local map in Lambert Conical projection for Fejokoo quadrangle. The rectangles correspond to close-up views of areas of interest: (a) Oxo crater, (b) Fejokoo and Sedana craters, (c) Kaneki crater and surrounding region, (d) Takel crater, (e) Jumi crater, (f) Cozobi crater and (g) Abellio and Victa craters.

2.4.4. The 3.43 and 4.0 μm absorption bands: carbonate abundances

In several areas on Ceres, the 4.0 μm carbonate band and the 3.43 μm absorption band are observed together, and they are positively correlated with high albedo areas, e.g Occator bright material (De Sanctis et al., 2016; Longobardo et al., 2017). In Fig. 11, the most prominent feature within the Fejokoo quadrangle is Oxo's ejecta followed by the material surrounding Takel crater (spectral profiles are shown in Fig. 12). The absorption band depths at 3.43 μm (Fig. 11A) and at 4.0 μm (Fig. 11B) were calculated by the technique described in (Combe et al., 2018). The data used for these two maps include all three orbital phases of the Dawn mission (Survey, HAMO and LAMO). These bands were interpreted as anhydrous carbonates by Rivkin et al. (2006), and the 4.0 μm carbonate band was observed by De Sanctis et al. (2016) on Occator bright materials (Longobardo et al., 2017; Palomba et al., 2018). An absorption band at 3.43 μm is also associated with aliphatic organics (De Sanctis et al., 2017), which create a positive spectral slope and lower the albedo (Schröder et al., 2017; Combe et al., 2018). A strong 3.43 μm absorption band can be interpreted as carbonates when it co-exists with a strong 4.0 μm absorption band and with a negative or neutral spectral slope.

Figs. 14–20 show regional maps of absorption band depth at 3.43 and 4.0 μm, illustrating the presence of carbonates in the Fejokoo quadrangle. The maps of band depths in Section 3 show the presence of a strong 3.43 μm absorption band in Oxo and Takel ejecta with a negative to neutral spectral slope and relatively high albedo, which we interpret as carbonates. The overall spectral slope of material in this quadrangle is negative to neutral, and thus there is no indication of organic materials. The fresh small craters at the lower latitudes of the

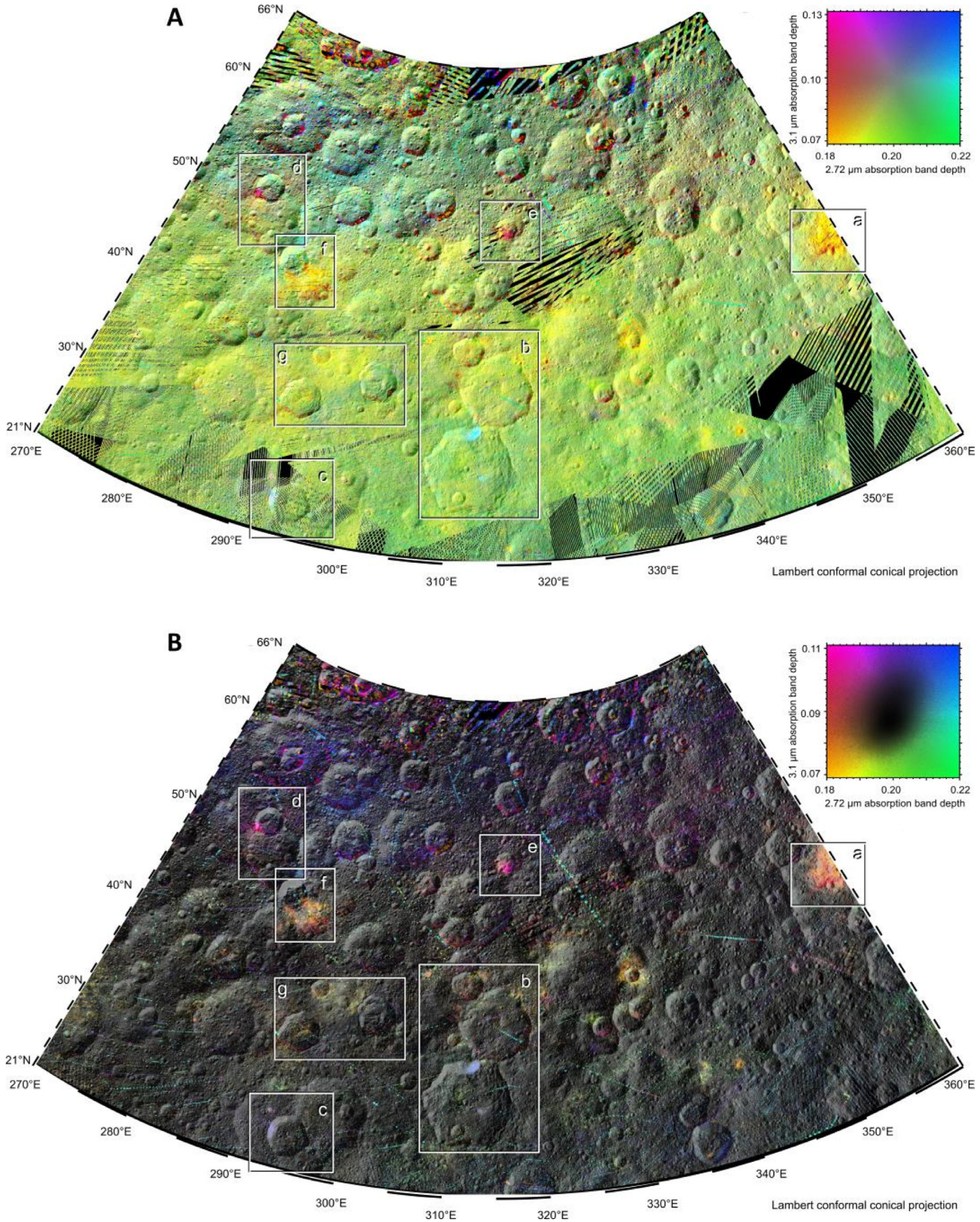

Fig. 10. Maps of the Fejokoo quadrangle showing the 2.72 μm band depth vs 3.1 μm band depth overlain on FC clear filter, using the color scheme described in Fig. 7(A) and using the color scheme described in Fig. 9(B). The rectangles correspond to close-up views of areas of interest: (a) Oxo crater, (b) Fejokoo and Sedana craters, (c) Kaneki crater and surrounding region, (d) Takel crater, (e) Jumi crater, (f) Cozobi crater and (g) Abellio and Victa craters.

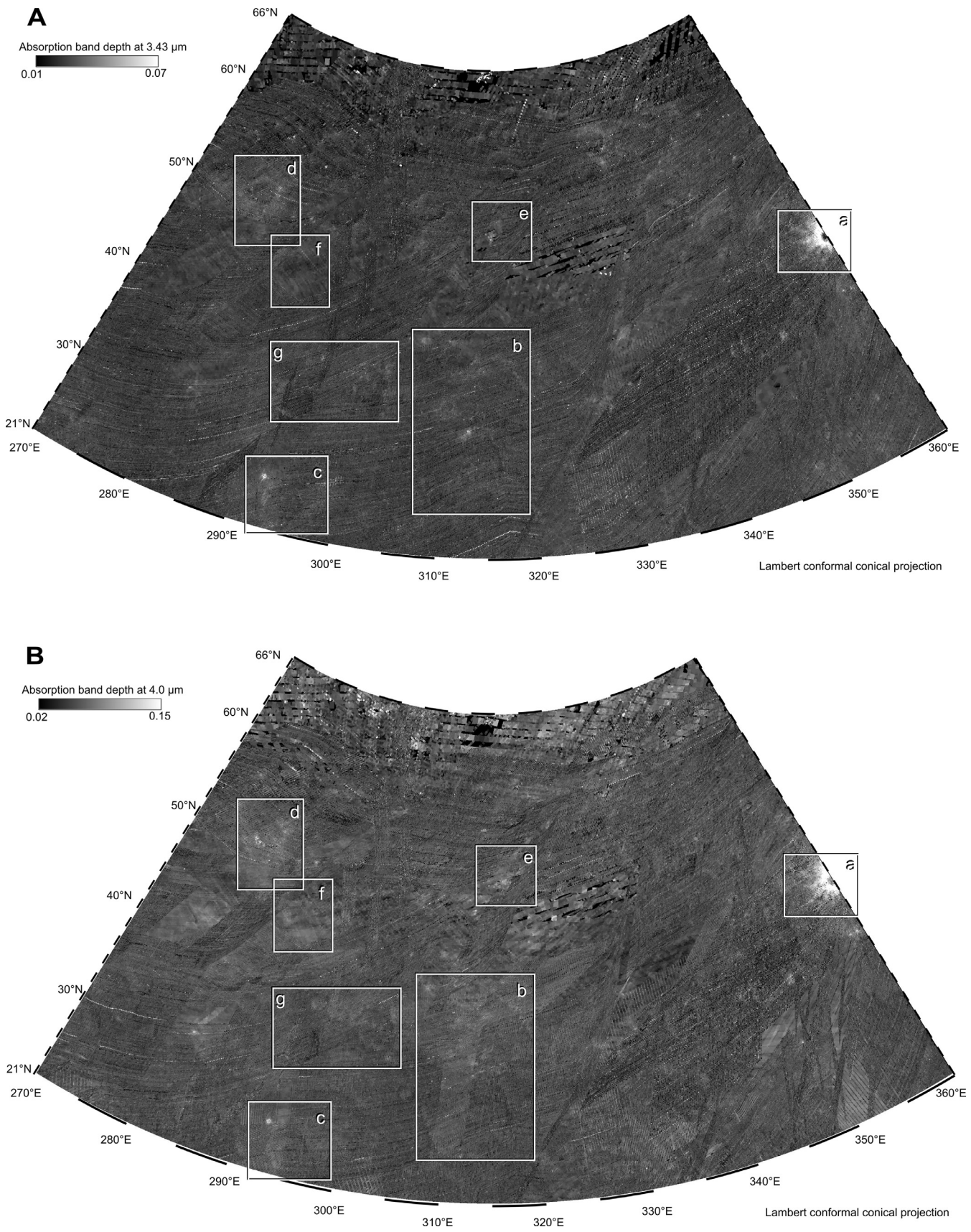

Fig. 11. Maps of the Fejokoo quadrangle showing the absorption band depth at 3.43 μm (A) and at 4.0 μm (B) from VIR observations. The rectangles correspond to close-up views of areas of interests: (a) Oxo crater, (b) Fejokoo and Sedana craters, (c) Kaneki crater and surrounding region, (d) Takel crater, (e) Jumi crater, (f) Cozobi crater and (g) Abellio and Victa craters.

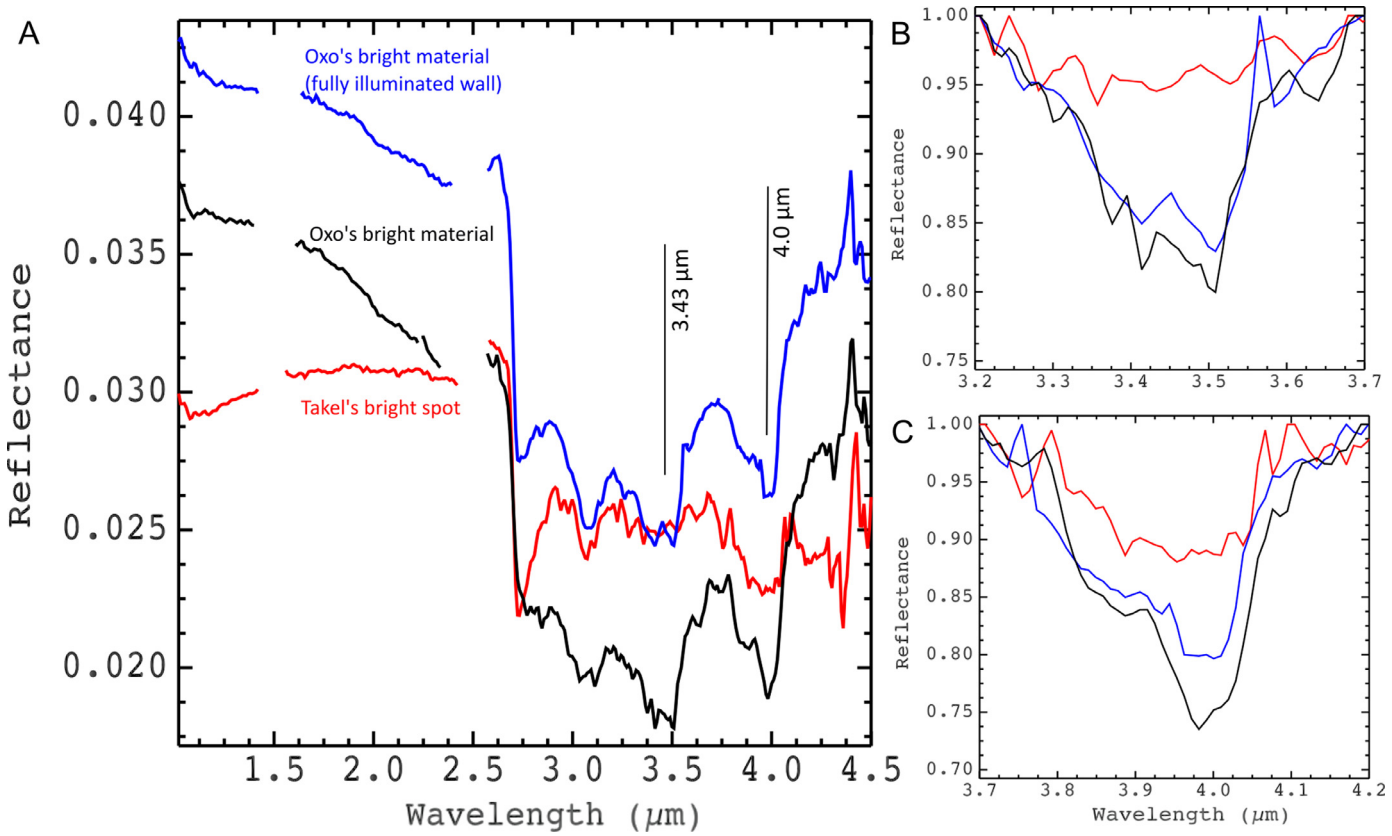

Fig. 12. (A) Spectral profiles from the bright material of Oxo (two different pixels illustrating the variation in reflectance within bright material) and Takel show that the 3.43 and 4.0 μm absorption bands are strong and spectral slopes between 1.0 and 2.5 μm are negative to neutral. (B) Close-up view of continuum-removed spectra highlighting the absorption band at 3.43 μm. (C) Close-up view of continuum-removed spectra highlighting the absorption band at 4.0 μm.

quadrangle and a crater adjacent to Fejokoo, named Sedana, (36.5°N, 314.7°E) also show a deep carbonate absorption feature. The 4.0 μm absorption band is apparent in pixels distributed along the craters walls and ejecta and is more apparent than the 3.43 μm absorption band (Fig. 3). The 4.0 μm absorption band is also found in some of the old craters and in the secondary crater chain towards the southeast of the quadrangle, suggesting that the carbonates at these locations are mixed with a dark component and a small amount of phyllosilicates.

2.5. Geological map

The Fejokoo quadrangle is dominated by heavily cratered terrain and represents a major fraction of the most densely cratered area on Ceres. The geological map of the Fejokoo quadrangle in Fig. 13 (Hughson et al., 2017) displays three distinct topographic provinces: a long, high aspect ratio region of considerably high topography along the western margin, a smaller quasi-circular region of moderately high topography in the northeast, and a large central low lying planitia dominated by degraded impact craters and six large, domical tholi. The Fejokoo quadrangle also hosts lobate material, lobate smooth material, and other crater and talus materials. In general, the spectra of all these regions, except lobate flows and bright materials, show variations in the band depth value of OH- and NH_4-phyllosilicate absorption features.

3. Mineralogical analysis of geologic units

In this section, we discuss the main compositionally distinct units of the Fejokoo quadrangle compared to the geological map shown in Fig. 13 and global spectral parameter maps of Ceres shown in Figs. 7 and 8. An overview of the compositional maps suggests a large mineralogical variation at regional scales and small variation across the quadrangle. A very important feature is undoubtedly Oxo crater and its ejecta material. In Oxo crater, we noticed very low values of both 2.72 and 3.1 μm band depth, and high albedo. The low absorption band depth values can imply several things such as low abundance of phyllosilicates, difference in grain size, phase changes such as dehydration resulting from impacts, variation in mineral abundance, and the heterogeneity of the external layers of both OH- and NH_4-bearing phyllosilicates (Ammannito et al., 2016). Two other similar locations were found near Cozobi crater's (42°N, 290°E) lobate flow and at Peko crater (38°N, 332°E) just north of the Aymuray tholi chain in the southeast of the quadrangle. In fact all the bright units in this quadrangle show low phyllosilicate absorption band depths.

3.1. Oxo (42.2°N 359.6°E)

Oxo is a bowl-shaped, ~10-km-diameter crater with unique surface composition that is the most prominent feature in the Fejokoo quadrangle. It is one of the youngest craters on Ceres (~3 Ma) with evidence of recent morphological changes (Jaumann et al., 2016; Hughson et al. 2017). The geology and morphology of Oxo are defined by four main units: the bright crater material, the smooth crater wall material, the smooth crater floor material, lobate material and the bright crater terrace material (Hughson et al. 2017; Combe et al., 2016). The northern wall of Oxo (Fig. 14A, B) is the second brightest feature on Ceres after the faculae of Occator crater (Stein et al. 2017; Schröder et al., 2017). High-albedo material covers the northern and eastern walls of the crater, part of the foot of the southern wall, part of the terrace and the well-defined ejecta blanket (Fig. 14B). Oxo's bright materials have a negative spectral slope in the infrared (Fig. 3) and visible (bluer, Fig. 12), whereas the rest of Ceres has a neutral or slightly positive spectral slope. Negative spectral slopes have been

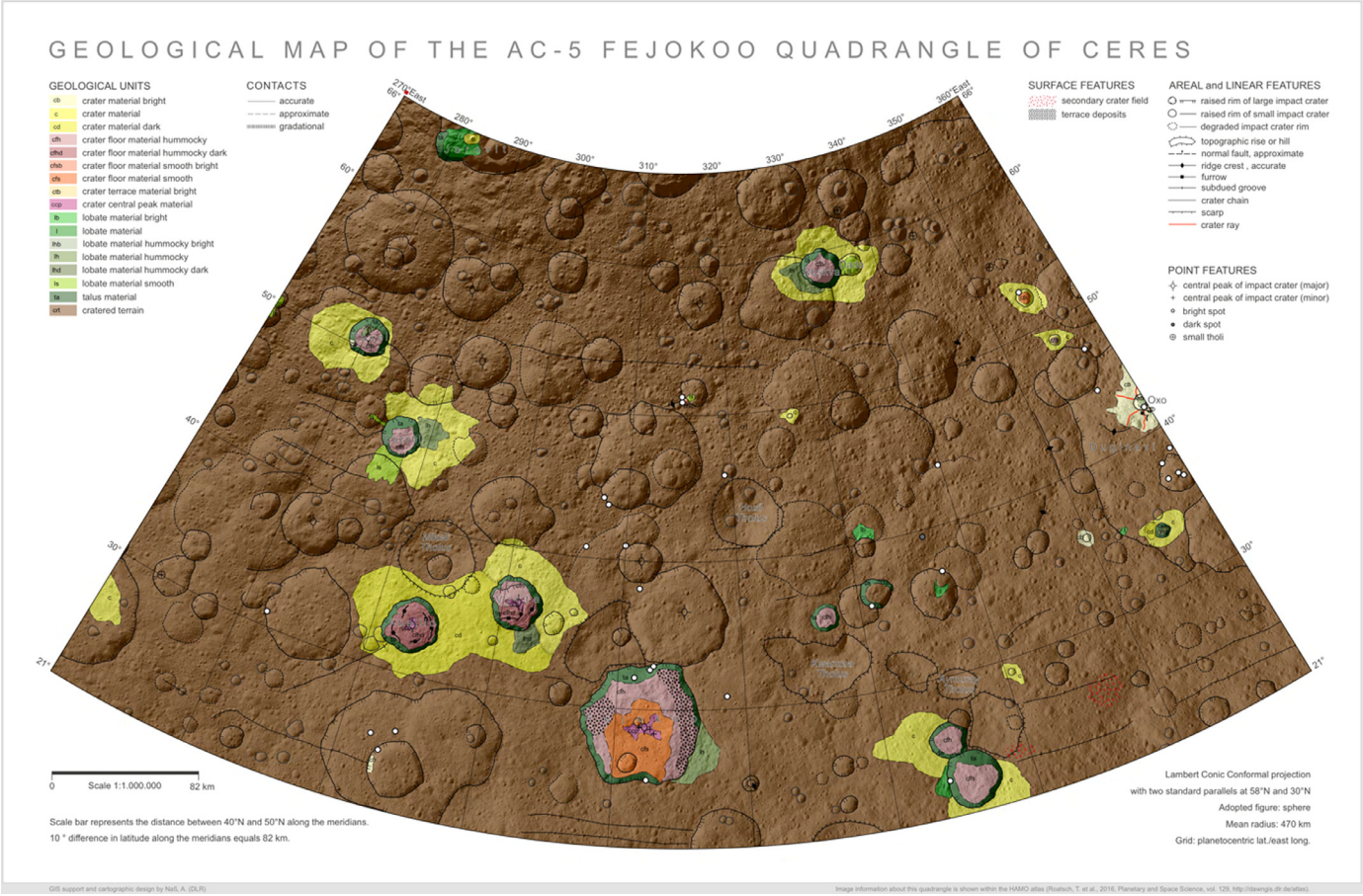

Fig. 13. Geological map of the Fejokoo quadrangle of Ceres featuring its main geological units, (Hughson et al., 2017).

associated with younger surface ages (Jaumann et al., 2016). H_2O ice was detected near the southern rim and corresponds to the high albedo materials on lobate mass-wasting deposits slumping to the floor of the crater (Combe et al., 2016; Hughson et al., 2017). This location is the only H_2O-rich area in the Fejokoo quadrangle (Combe et al., 2018). An example spectrum from this area exhibits absorption bands at 1.65 and 2.0 μm (Fig. 3); these bands are most likely due to freshly exposed surface ice (Hughson et al., 2017; Combe et al., 2016, 2018). Spectra of other locations in the Fejokoo quadrangle are shown for comparison in Figs. 3 and 12.

The surface composition of all the units in Oxo are distinct both within the Fejokoo quadrangle and compared to Ceres' global composition. The bright material surrounding the crater and its floor material are characterized by low abundances of hydroxylated (OH) and ammoniated (NH_4) phyllosilicates, compared to the global composition. Conversely, absorption band depths at 3.43 and 4.0 μm of carbonate minerals are deep and cover the entire Oxo ejecta blanket (Fig. 14F, G). However, on the floor of Oxo, the absorption bands at 3.43 and 4.0 μm are weaker: the 3.43 μm absorption band is absent whereas the 4.0 μm absorption band is deep and prominent. The absence of the 3.43 μm band absorption on the floor corresponds to the H_2O-rich area, and the broad OH absorption band at 3.0 μm is probably masking the 3.43 μm carbonate band (Fig. 12).

3.2. Fejokoo and Sedana craters (Center: 29.1°N, 312.1°E)

Fejokoo crater (Fig. 15A) is the largest crater in the Fejokoo quadrangle; it is hexagonal in shape and equilateral. It is ~68 km diameter with steep walls and a flat floor. The crater was formed in the intermediate stratigraphic period after the formation of Ceres (Hughson et al., 2017). Two bright material locations (Fig. 15B–E), bright streaks (30°N, 313°E) on the northern crater wall and a smaller area east of the central peak, both displayed in blue (Fig. 15C, D, H), show strong 2.72 and 3.1 μm absorption band depths indicating the occurrence of OH-rich and NH_4-rich phyllosilicates (Fig. 15C, D, H). Otherwise the composition of Fejokoo is similar to the global composition of Ceres (Figs. 7, 8, 10 and 15C), in spite of its complex geology (Fig. 13). The 3.43 and 4.0 μm carbonate absorption bands are relatively weak, but they are detected. (Fig. 15F, G). A relatively strong 4.0 μm absorption band extends to the adjacent crater, Sedana (36.5°N, 314.7°E) towards the north and covers the entire east-facing wall along with the smaller crater to the north.

Sedana crater has low abundances of both OH and NH_4 phyllosilicates. The rim of Sedana has a very low 2.72 μm absorption band depth compared to the surrounding terrain suggesting heterogeneity in the stratigraphic layer during its formation (see detailed interpretation of a similar case in Combe et al., 2018). The albedo of this area (Fig. 15B) is relatively low compared to other bright areas in this quadrangle suggesting that carbonates and phyllosilicates are mixed at various concentrations within the quadrangle. The crater's visible spectrum has an overall negative spectral slope (Fig. 15E) except for the bright spots (Fig. 13) that have a slight positive spectral slope (Fig. 15E), and relatively deeper carbonate bands.

3.3. Kaneki crater (23.8°N, 294.6°E) and surrounding region

Kaneki crater (31.5 km diameter) is southwest of Fejokoo crater. Its western rim has multiple bright areas identified in the geological map (Fig. 13, Hughson et al., 2017) that are visible in the photometrically corrected, albedo map (Fig. 16B). The region of the bright areas, the

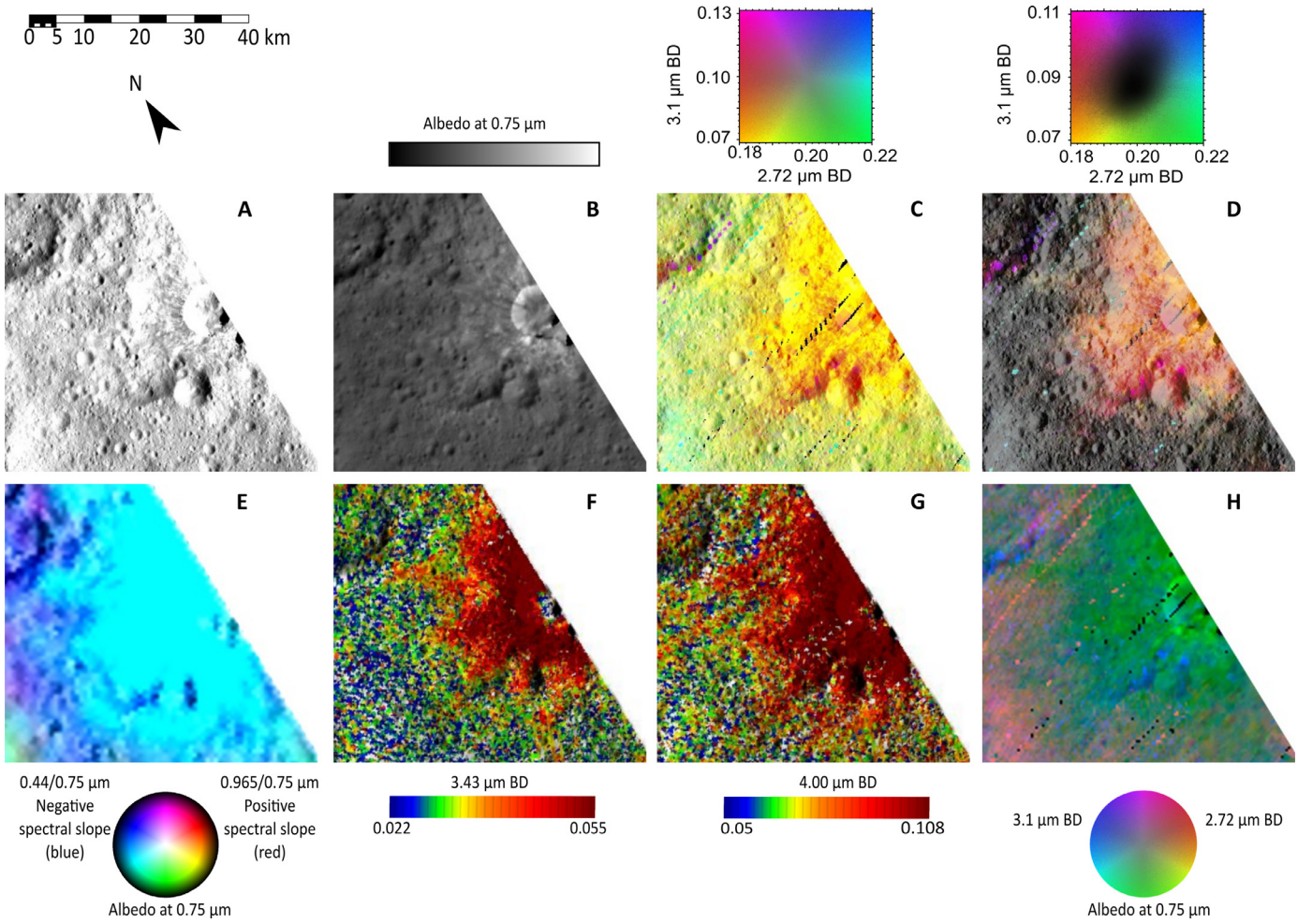

Fig. 14. Regional maps of Oxo and its ejecta blanket. (A) FC clear filter LAMO, from Fig. 1 bottom (B) FC photometrically-corrected map, from Fig. 2A (C) 2.72 and 3.1 μm band depths indicative of low abundance of phyllosilicates using color scheme from Fig. 9B and (D) same as C overlain on FC clear filter per Fig. 10 (E) color composite same scheme as Fig. 5, (F) 3.43 μm absorption band depth, (G) 4.0 μm absorption band depth (H) color composite same scheme as Fig. 6. All these maps are illustrated here to compare various spectral parameters of the same region in Fejokoo quadrangle.

western crater rim, has a strong 3.1 μm absorption band of NH_4 phyllosilicates, moderately deep 2.72 μm band (Fig. 16C, D, H), and relatively strong 3.43 (Fig. 16F) and 4.0 μm (Fig. 16G) carbonate bands, indicating a mixture of phyllosilicates and carbonates with relatively smaller amounts of dark material compared to the surrounding region. Overall the albedo of this region is relatively higher than surrounding terrains, with slightly positive spectral slope (yellow-green in Fig. 16E).

A small, fresh crater northwest of Kaneki stands out in all parameters displayed in Fig. 16 and lies inside a larger, degraded crater. It has the same albedo and spectral slope (Fig. 16E) as Kaneki's western crater rim, though the phyllosilicate composition is higher in NH_4 compared to OH as seen in Fig. 16C, D, H. Both carbonate bands are deep in this small crater (unnamed to date).

3.4. Takel crater (50.7°N, 280.6°E)

Takel is a 22-km diameter, well-preserved crater in the northwest region of the Fejokoo quadrangle. Hughson et al. (2017) report an asymmetric rim and a moderately sized mass-wasting feature on the northern crater floor. Another apparently mass-wasted area falls outside of the south-western rim and is distinct in spectral parameters (Fig. 17). Takel crater deviates from the mean composition in this quadrangle as shown in Fig. 17A–H. The composition of the mass-wasted materials from the southwest crater rim is consistent with higher concentration of NH_4 phyllosilicates (Fig. 17C, D, H) relative to OH-bearing phyllosilicate. There is a clear boundary where the 3.1 μm band depth is weaker towards the north-east region of the crater floor and the 2.72 μm band is deep (Fig. 17C, D, H) as compared to other regions around the crater. Carbonate absorption bands (Fig. 17F, G) are weak to moderate on the crater's floor, whereas they are stronger on the northwest crater wall compared to elsewhere in and around the crater, with different relative band depths. The spectra of Takel's bright material are shown in Fig. 3 with a close-up view of the phyllosilicate bands and in Fig. 12 with a close-up view of the 3.43 and 4.0 μm absorption bands. The overall albedo of the bright material in the crater is relatively higher than the albedo of the Fejokoo quadrangle, with a negative spectral slope (Fig. 17E). The material with 3.43 and 4.0 μm absorption bands (Fig. 17F, G) surrounds the crater and corresponds to ejecta material.

3.5. Jumis crater (51.6°N, 316.4°E)

Jumis crater (~15-km diameter) has a distinctive surface composition with some similarities to Takel crater, and both are located at the same latitude. Its surface, like Takel crater, has lobate smooth material starting from the rim of the impact crater and running downslope, continuing further towards the center of a larger crater to the southwest as can be seen in Figs. 1 and 12). This larger crater is only partially seen in the lower left corner of Fig. 18A–B. This flow is thought to have formed, either directly or indirectly, as impact-triggered landslides

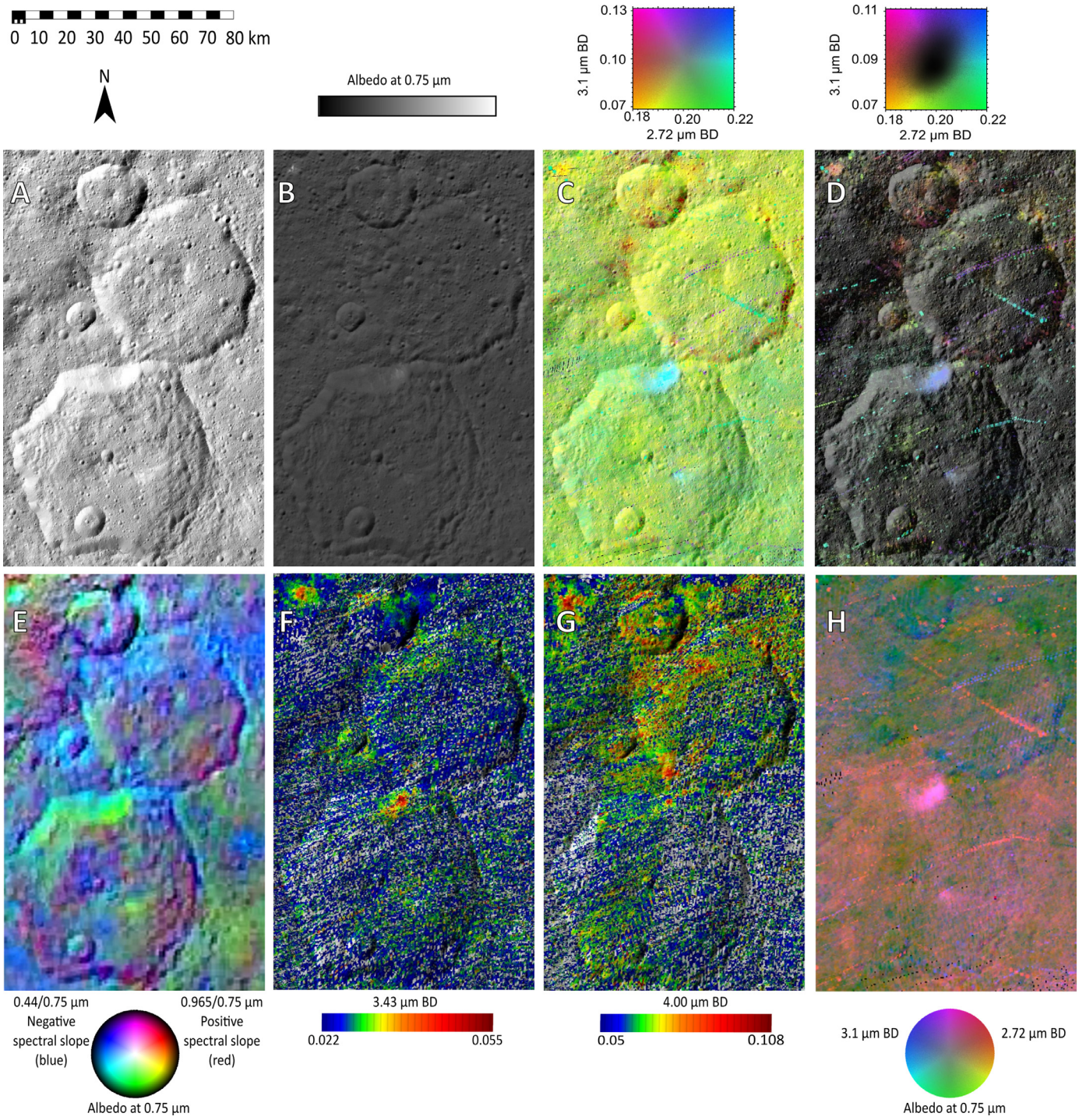

Fig. 15. Regional maps of the Fejokoo and Sedana craters. (A) FC clear filter LAMO B) FC photometrically corrected map, (C) & (D) 2.72 and 3.1 µm band depth maps using same scheme as Figs. 7 and 10, (E) Color composite same scheme as Fig. 5, (F) 3.43 µm absorption band depth map, (G) 4.0 µm absorption band depth map (H) color composite same scheme as Fig. 6.

(Hughson et al., 2017). The overall composition of ejecta is similar to the global composition of Ceres with both OH and NH_4 phyllosilicates present (Fig. 18C, D, H). However, the ammoniated phyllosilicates seem to have high abundance just south of the lobate flow and crater wall, around a small crater located on the southern wall of Jumis, (Fig. 18C, D, H). This southern area is characterized by a positive spectral slope and slightly higher albedo than surrounding terrains (Fig. 18E). The ammoniated phyllosilicates may be exposed as a result of the fresh impact on the walls of the older crater. The two carbonates bands at 3.43 and 4.0 µm (Fig. 18F, G) co-exist around the smaller crater on the southern wall of Jumis. The region of slightly higher abundance of carbonate (Fig. 18F, G) extends across Jumis crater and trends north-eastward.

3.6. *Cozobi crater (45.3°N and 287.3°E)*

The Cozobi crater (24 km diameter) region has unique geomorphological features (Fig. 19A), with an asymmetric crater rim and collapsed southern rim indicating extensive mechanical failure of the crater wall. Impact ejecta is deposited north and east of the crater

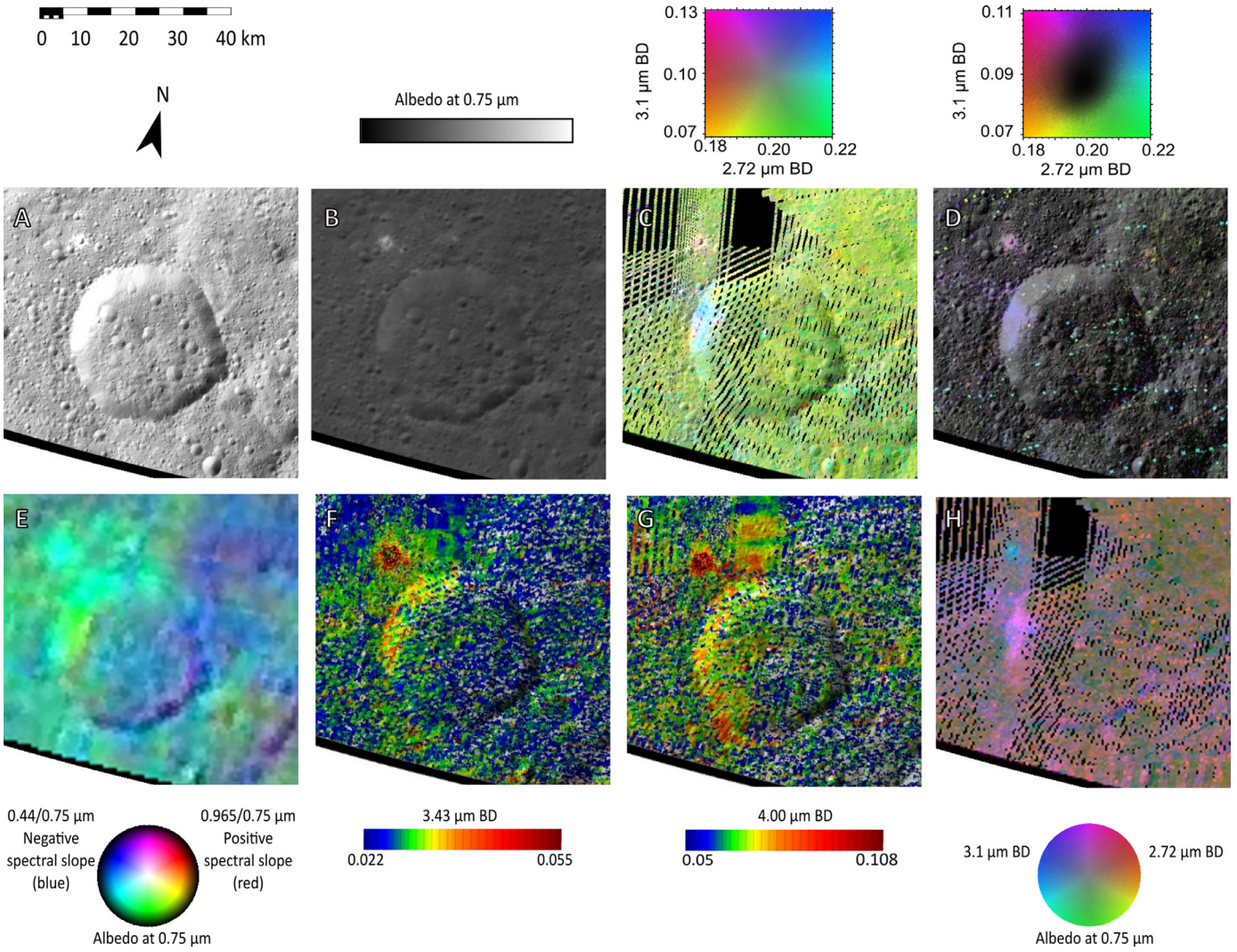

Fig. 16. Regional maps of the Kaneki crater centered at 23.8° N, 294.6° E. (A) FC clear filter LAMO (B) FC photometrically corrected map, (C) & (D) 2.72 and 3.1 μm band depth maps using same scheme as Figs. 7 and 10, (E) Color composite map same scheme as Fig. 5, (F) 3.43 μm absorption band depth map, (G) 4.0 μm absorption band depth map, (H) color composite with same scheme as Fig. 6.

(Fig. 19A); two lobate flow features are also seen emanating radially away from the southern and western walls (Fig. 13, and Hughson et al., 2017), which are possibly associated with the collapsed rim. The most striking mineralogical feature is that of the lobate flow (Fig. 19C, D, E, H), which has low-abundance in both OH and NH_4 phyllosilicates, slightly higher albedo than surrounding terrains (Fig. 19E, H), and spectra with a negative overall slope (Fig. 19E). These characteristics are similar to those of Oxo's ejecta flows; however, the carbonate bands are weaker than those of Oxo's ejecta (Fig. 19F, G), despite the high albedo. There are a few locations on and off the lobate flow where the 4.0 μm absorption band is strong, but it doesn't follow the lobate flow in general (Fig. 19A, G)). The absorption band depth at 3.43 μm (Fig. 19F) is quite low and doesn't correlate to the 4.0 μm absorption band depth. Because of that, we do not consider this area to be rich in carbonates. The ejecta towards north of the rim (cyan in Fig. 19C, D) has a deeper OH-phyllosilicate band at 2.72 μm and moderately deep NH_4 phyllosilicate band at 3.1 μm compared to the lower values of the lobate flows. It is likely that the ejecta pre-dates the formation of the lobate flow. Note that the crater floor material is more NH_4-rich compared to OH in the phyllosilicates and is closer to the spectral characteristics of the ejecta material in all parameters presented in Fig. 19.

3.7. Abellio crater (33.2°N and 293.2°E) & Victa crater (36.2°N and 301.1°E)

Abellio and Victa are two distinct craters, possibly formed during the oldest stratigraphic period of Ceres (Hughson et al., 2017). They have similarities in composition and morphological features. Abellio is ~ 32 km in diameter with a topographically asymmetric floor displaying concentric ridges and terraces that are morphologically similar to those found in craters on icy satellites (Hughson et al., 2017; Schenk, 1989). Victa crater is also ~ 32 km in diameter and is located just east of Abellio, with steep walls, evidence of mass wasting and ridges within the crater floor. The surfaces of both Abellio and Victa exhibit lower albedos (Fig. 20B) than the average of the Fejokoo quadrangle, and negative spectral slope for the ratio at 0.44/0.75 μm (Fig. 20E). The general composition is similar to the global composition of Ceres with low band depth values of OH and NH_4 phyllosilicates (Fig. 20C, D). The composition of the northern region in Fig. 20 is influenced by the Mikeli tholus (Figs. 1, 3, 12, and 20C, D, H) indicating slightly lower abundances of hydroxylated (OH) phyllosilicates than the area within and between the two craters. The area between Victa and Abellio has lower albedo and similar mineralogy to the floors of the two craters. The southern ejecta from these two craters have slightly higher albedo than the floors of the crater with low OH and NH_4 phyllosilicates band

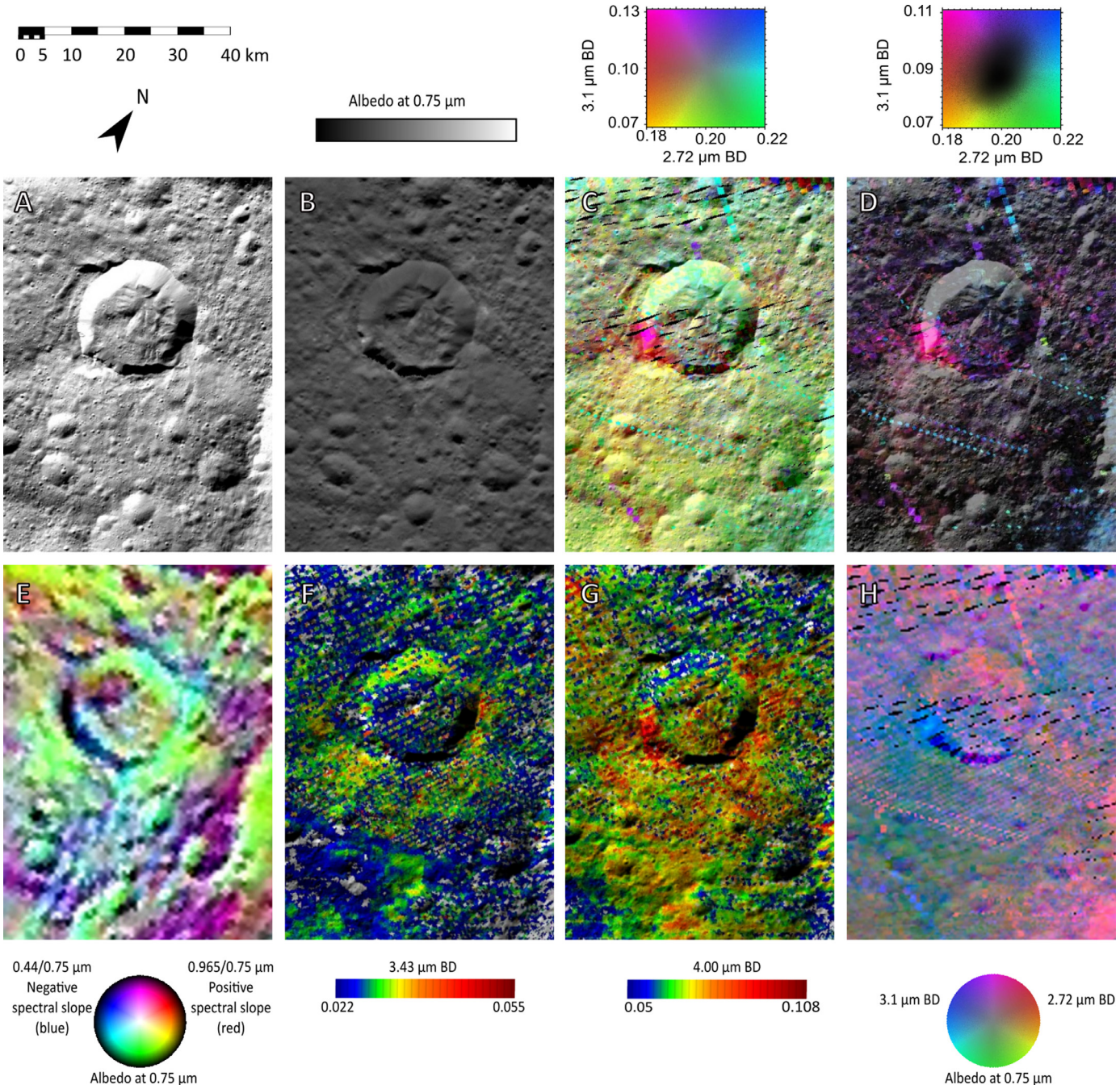

Fig. 17. Regional maps of Takel crater centered at 50.7° N, 280.6°E. (A) FC clear filter LAMO, (B) FC photometrically corrected map, (C) & (D) 2.72 and 3.1 μm band depth maps using same scheme as Figs. 7 and 10, (E) Color composite with same scheme as Fig. 5, (F) 3.43 μm absorption band depth map, (G) 4.0 μm absorption band depth map, (H) color composite with same scheme as Fig. 6.

depths. The absorption band depths of carbonates at 3.43 (Fig. 20F) and 4.0 μm (Fig. 20G) are low in this region, showing little to no lateral variation in carbonates in the regions not affected by Mikeli tholus. A low abundance of carbonates is consistent with the lower albedo relative to the quadrangle average and suggests the presence of more abundant dark material that might mask carbonate bands.

3.8. *Tholus material*

There are a total of six tholi or domical mountains within the Fejokoo quadrangle (Fig. 1, 12). Aymuray tholi comprise a chain of three different tholi centered at 29°N, 336°E (Hughson et al., 2017). These share many morphometric and geographical similarities with the cryovolcanic structure Ahuna Mons (Ruesch et al., 2016; Hughson et al., 2017; Zambon et al., 2017). Three tholi (Mikeli (38.6°N, 293.6°E), Hosil (43.2°N, 320.8°E), and Kwanzaa (32.2°N & 326.5°E)) have similar surface compositions though they differ from the surrounding cratered terrains as seen in Figs. 3 and 10. All the tholi have weaker 2.72 and 3.1 μm absorption band depths than the overall global composition of phyllosilicates. The carbonate absorption band depths at 3.43 and 4.0 μm are also weak at these locations (Fig. 3). The spectral slope is negative to neutral (Figs. 3 and 5) compared to the average. Dark material dominates the overall composition of these areas; regions with slightly higher albedo have noticeably more negative spectral slopes. Although the Aymuray tholi have similar composition as the other three tholi, this complex is richer in OH phyllosilicates, with

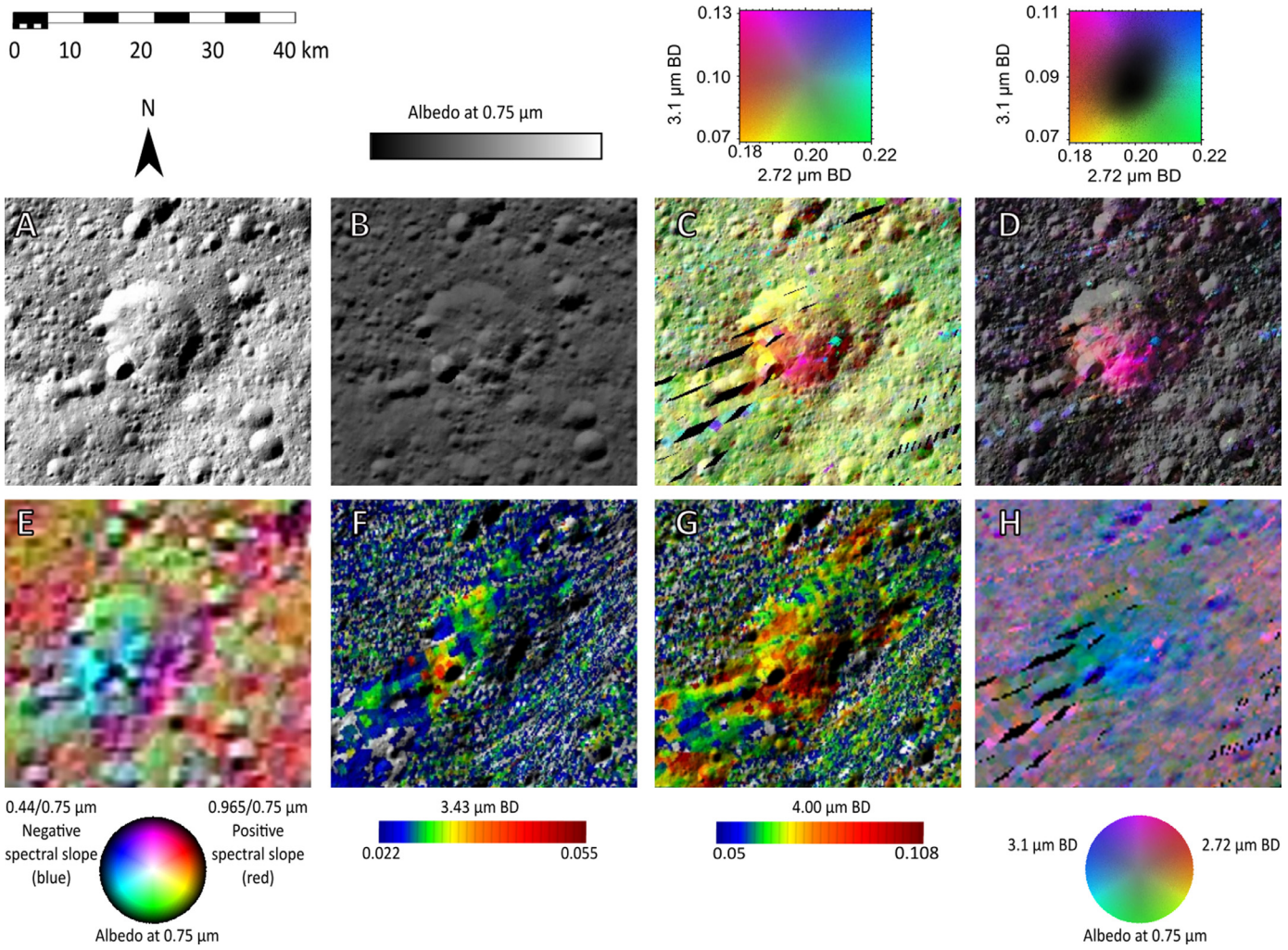

Fig. 18. Regional maps of the Jumis crater centered at 51.6° N and 316.4° E. (A) FC clear filter LAMO (B) FC photometrically corrected map, (C) & (D) same as Fig. 10 focused on Jumis crater. (E) False color maps same as Fig. 4, (F) 3.43 μm absorption band depth map, (G) 4.0 μm absorption band depth map, (H) color map same as Fig. 6.

slightly positive spectral slopes and higher albedo than the others. In the flat plains east of Aynuray tholi, several small craters have higher abundances in both OH and NH_4 phyllosilicates and carbonates. A clear carbonate (4.0 μm) distribution boundary can be seen in the southern region; it may be due to the ejecta material from the craters Halki (~26°N, 335°E) and Telepinu (23°N, 336°E).

4. Discussion

4.1. Distribution of OH-rich and NH_4-rich phyllosilicates

The overall presence of phyllosilicates within the Fejokoo quadrangle supports the interpretation that surface materials were altered by aqueous processes during early stages of the formation of Ceres. However, we observed variations in the band depths of OH and NH_4 phyllosilicate spectra. Absorption band depth can be indicative of various factors, including abundance, grain size, and mineral composition and phase change. Consequently, measurements of absorption band depth variations may reflect the lateral heterogeneity of the external layers of the surface (Ammannito et al., 2016). The shallower absorption bands in the ejecta material and near fresh craters suggests that impact heating could have been responsible for lower abundances of phyllosilicates near craters (e.g. Oxo and Takel craters). However, there are several locations where NH_4 phyllosilicates seem to surround some of the fresh small craters, which may suggest that different dehydration or alteration processes are involved, and that impact heating alone may not be the cause of the spectral variations. The lack of correlation between the depths of hydroxylated and ammoniated bands at different locations within the quadrangle also suggests that these minerals can react to different formation conditions. There are locations (i.e. Fejokoo's bright materials) with high abundances of both OH and NH_4 phyllosilicates. These areas can be interpreted in terms of relatively higher mineral abundance and perhaps those regions are younger than the heavily cratered terrain that dominates the Fejokoo region (Fig. 13). Some other processes such as landslides may have either exposed minerals of varying composition from the sub-surface or effected a phase change due to local changes in temperature and pressure conditions.

4.2. Distribution of carbonates

Carbonates are observed in the Fejokoo quadrangle, indicative of aqueous alteration processes; they seem to be found associated with the bright crater ejecta and are anti-correlated with the abundance of phyllosilicates, as observed for all the detected bright spots on Ceres (Palomba et al., 2018). At some locations, the ratio of 3.43 and 4.0-μm absorption band depth is not constant, which may suggest different compositions of carbonates and thus different origin and evolution (e.g. Carrozzo et al., 2018). Different types of carbonates can be excavated by impact craters from multiple layers beneath the surface. The

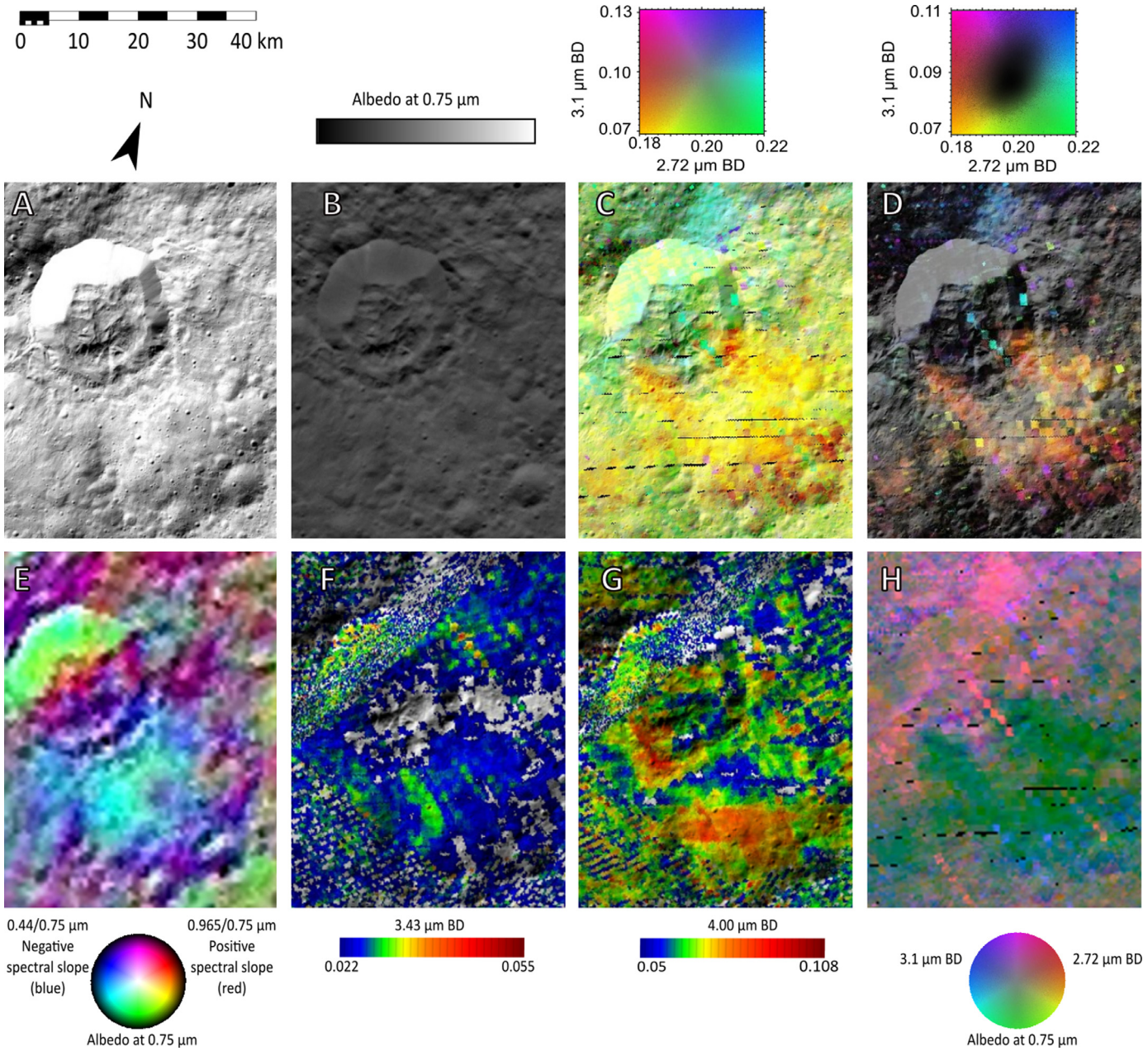

Fig. 19. Regional maps of Cozobi crater. (A) FC clear filter LAMO (B) FC photometrically corrected map, (C) & (D) same as Fig. 10 focused on Cozobi Crater (E) False color maps same as Fig. 4, (F) 3.43 µm absorption band depth map, (G) 4.0 µm absorption band depth map, (H) color map same as Fig. 6.

observed range of carbonate absorption band depths is indicative of a variety of chemical alteration processes and provides evidence that aqueous alkaline solutions have persisted in Ceres at global scales. The 4.0 µm carbonate band is detected everywhere on the surface of Ceres (Carozzo et al., 2018). Small areas with low abundance of carbonates have generally high abundances of phyllosilicates and relatively lower albedo. The observed extensive carbonate deposits imply earlier layers of brine-rich liquids or subsurface ocean of regional extent.

4.3. Absence of organic materials

The 3.43 µm absorption band depth used in this study is theoretically sensitive to both carbonates and aliphatic organics (De Sanctis et al., 2017). We do not detect any organics in the Fejokoo quadrangle. Even though the 3.43 µm absorption band is detected throughout the entire quadrangle, it is always associated with the 4.0 µm absorption band of carbonates. The organics detected on Ceres (De Sanctis et al., 2017) appear reddish in color (positive spectral slope) (Pieters et al. 2017; Schröder et al., 2017). Understanding the positive spectral slope may constrain the presence of organics. Although we do observe red to orange pixels in the northern latitudes in Fig. 5, indicative of positive spectral slopes, they are not correlated with the 3.43 µm absorption band. The red - brown pixels in the northern latitudes displayed in Fig. 5, are due to the high incidence angle and fall within the uncertainty limits and are thus artifacts of the lighting conditions during data acquisition. The trend of more positive spectral slopes towards higher latitudes cannot be interpreted in terms of surface composition.

4.4. Interpretation of surface composition in the geological context

Hughson et al. (2017) presented a geological history of the Fejokoo quadrangle, estimated the relative age of impact craters, and interpreted the stratigraphic period of their formation. Based on

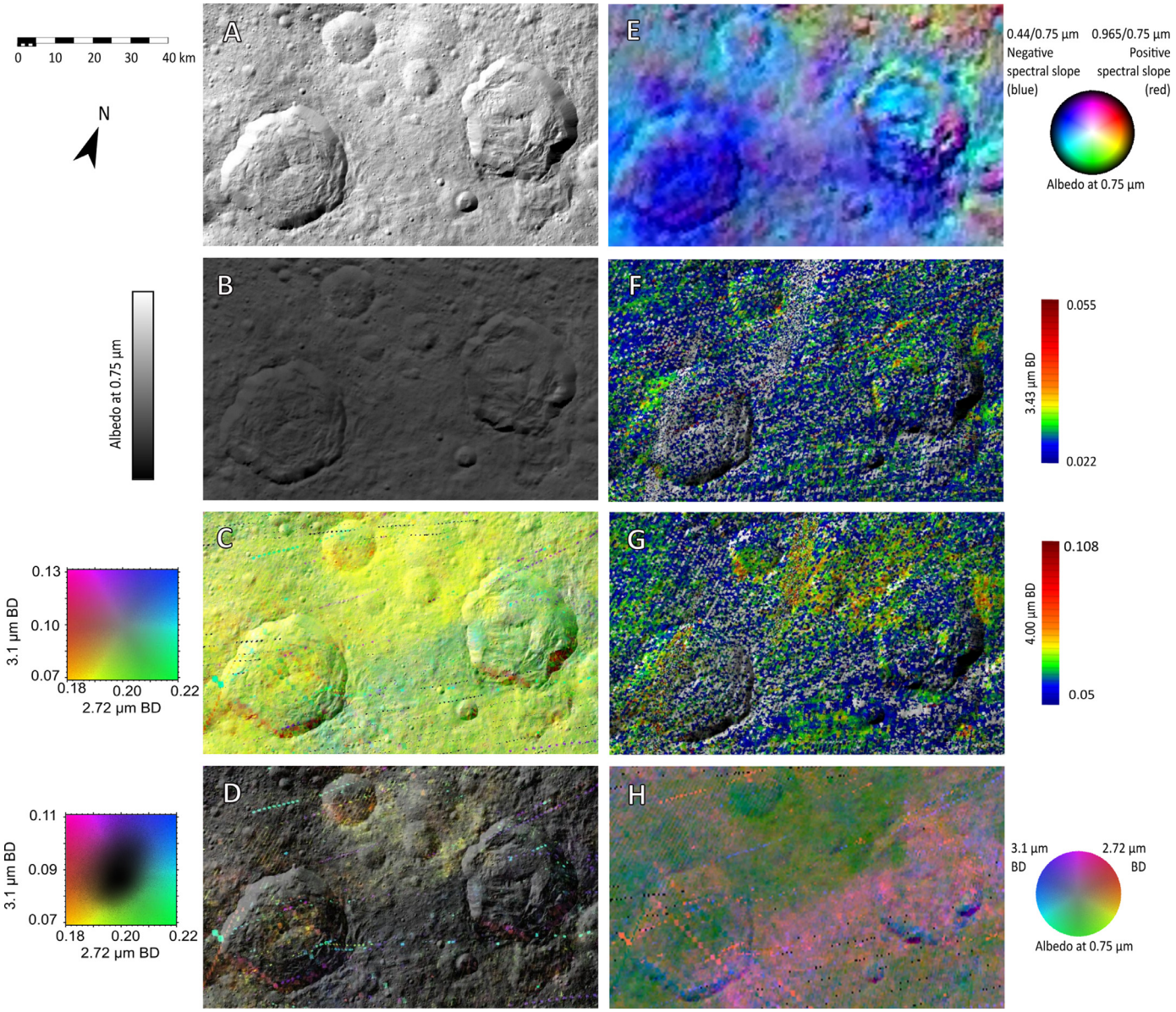

Fig. 20. Regional maps of the Abellio and Victa crater region including Tholus. (A) FC clear filter LAMO (B) FC photometrically corrected map, (C) & (D) same as Fig. 10 but localized at Abellio and Victa crater region (E) False color maps same as Fig. 4, (F) 3.43 µm absorption band depth map of the Abellio and Victa region, (G) 4.0 µm absorption band depth map of the Abellio and Victa region, (H) color map same as Fig. 6.

morphological freshness and impact crater densities, the Fejokoo quadrangle is broadly divided into four geological periods which from oldest to youngest are termed the "Oldest period", "Intermediate period", "Young period" and "Youngest period" (Fig. 17, Hughson et al., 2017). Oxo falls within the youngest period, Abellio, Victa, and Takel belong to the young category, and Fejokoo belongs to the Intermediate period. Although we attempted to find a mineralogical reference to this chronology and identify common spectral features related to the stratigraphic periods, no such relationship in the surface composition was identified. For example, Takel crater's composition (a crater high in carbonates formed in the Young stratigraphic period) is somewhat similar to Oxo's ejecta, which formed during the Youngest stratigraphic period. Furthermore, Takel has a high abundance of NH_4 phyllosilicates while Oxo lacks phyllosilicates. Conversely, Cozobi's mass wasting features are poor in phyllosilicates, similar to Oxo's ejecta, and poor in carbonates. Even though these craters are at similar latitudes, their composition is determined by the subsurface and the subsurface seems to be different within the quadrangle. The difference in phyllosilicate and carbonate composition in the craters from the same stratigraphic period implies that Ceres' subsurface materials may have undergone different types of aqueous alteration and chemical reactions at different locations. The subsurface may have significant regional differences within the Fejokoo quadrangle.

4.5. Comparison with regions outside of the Fejokoo quadrangle

The Fejokoo quadrangle shows variations in composition that are also prominent at the global scale. Oxo and the low albedo region of Abellio and Victa craters are particularly distinctive. Oxo has similarities with Occator (De Sanctis et al., 2016), such as high albedo materials (Occator faculae are the brightest materials on Ceres) and high abundances of carbonates. However, Oxo's OH-phyllosilicate-poor and NH_4-phyllosilicate-poor ejecta is completely different from Occator's OH-rich and NH_4-rich ejecta (e.g. Longobardo et al., 2017; Combe et al., 2018). Conversely, the albedo of Occator's ejecta is somewhat similar to Abellio and Victa crater material, but both regions differ in surface

composition, supporting the hypothesis that different sublayers were excavated to produce the observed surface (Ammannito et al., 2016). Overall, the ubiquitous presence of phyllosilicates and the multiple detections of carbonates associated with fresh impact craters supports the hypothesis that intense hydrothermal processes once occurred on Ceres, as a strong indicator of the widespread presence of H_2O on the surface or in the subsurface at the time of their formation.

5. Conclusion

Mineralogical analysis of the Fejokoo quadrangle of Ceres has been performed using maps calculated from Dawn's VIR mapping spectrometer data and images from the Framing Camera. We identified several locations with surface composition that varies significantly from Ceres' global composition. (1) The northern walls and ejecta of Oxo crater are the second brightest areas on Ceres after Occator; similarly, Oxo's crater walls have low abundance of OH-bearing materials and are enriched in carbonates, (see also Palomba et al., 2018). (2) Spectra of the ejecta of Takel crater are also consistent with the presence of carbonates, although the distribution of absorption bands at 3.43 and 4.0 μm suggests different origins for the carbonates and differences in the composition of subsurface layers at northern and southern latitudes with in the Fejokoo quadrangle. (3) Small and young craters at lower latitudes within the Fejokoo quadrangle are rich in both OH and NH_4 phyllosilicates and in carbonates, suggesting fresh material was excavated from different subsurface layers further to the north. The presence of carbonates and the variation in the intensity of absorption features on the surface indicates aqueous alteration of the surface materials. An impact results in excavating materials deeper near the center of the cavity, and the variation in composition of the distributed ejecta also reflects differences in the underlying stratigraphy; materials ejected to larger distances from the impact originate from the deepest parts of the impact site. The presence of these minerals and their distribution along geological features requires the right thickness of stratification and depth of the impact to produce observed differences at the surface. Variation in carbonate composition implies a past, subsurface ocean when the brine-rich material was liquid.

The dominant geologic process within the Fejokoo quadrangle is undeniably impact cratering. The observed compositional diversity is mainly observed in correspondence with crater material units as well as with lobate deposits associated with fresh impact craters. Overall, the northern latitudes show a small range of spectral variations compared to the purest and most extreme compositions detected on Ceres. However, the spectral variations observed within this region are consistent with moderate lateral compositional variations. The occurrence of high albedo along with phyllosilicates and carbonates bands is limited to fresh, small craters. Other major geological features such as lobate flows, and ejecta material have high albedo with either phyllosilicates or carbonates, but not both. The overall surface composition within the Fejokoo quadrangle is relatively homogeneous and similar to the average composition of Ceres. This can be interpreted as the occurrence of the geological processes that were on average the same as on Ceres.

We did not find systematic variations of the two phyllosilicate absorption bands and both carbonate bands in association with any major geological unit such as large craters, crater material, tholi, or lobate material. However, fresh, small craters in the southern latitudes are characterized by strong absorption bands of phyllosilicates at 2.72 and 3.1 μm and of carbonates at 3.43 and 4.0 μm, which was the focus of this study. As a corollary, evidence of alteration of the dominant materials is indicated by reduced strength of the primary absorption band depths in this study that exists on most of the Fejokoo region and elsewhere on Ceres.

Acknowledgments

We thank the Italian Space Agency (ASI-INAF n. I/004/12/1) and NASA for supporting this work. The VIR instrument was funded and coordinated by the ASI and built by Selex ES, with the scientific leadership of the Institute for Space Astrophysics and Planetology, Italian National Institute for Astrophysics, Italy. The VIR is operated by the Institute for Space Astrophysics and Planetology, Rome, Italy. A portion of this work was carried out at the Jet Propulsion Laboratory, California Institute of Technology, under contract to NASA. Dawn data are archived in NASA's Planetary Data System; VIR spectral data may be obtained at https://sbn.psi.edu/pds/resource/dwncvir.html, last accessed 2018 January 17.

Supplementary materials

Supplementary material associated with this article can be found, in the online version, at doi:10.1016/j.icarus.2018.08.025.

References

Ammannito, E., et al., 2016. Distribution of phyllosilicates on Ceres. Science 353 (6303) aaf4279.

Carrozzo, F.G., Raponi, A., Sanctis, M.C., Raponi, A., Ammannito, E., Giardino, M., D'Aversa, E, Fonte, S., Tosi, F., Capaccioni, F., Capria, M.T., Ciarniello, M., Longobardo, A., Palomba, E., Zambon, F., Russell, C.T., Raymond, C.A., 2016. Artefacts removal in VIR/DAWN data. Rev. Sci. Instrum. 87, 124501. 10.1063/1.4972256.

Carrozzo, F.G., et al., 2018. Nature, formation and distribution of carbonates on Ceres. Sci. Adv. 2018 (4), e1701645.

Carry, B., Dumas, C., Fulchignoni, M., Merline, W.J., Berthier, J., Hestroffer, D., Fusco, T., Tambly, P., 2008. Near-infrared mapping and physical properties of the dwarf-planet. CeresA&A 478, 235–244. https://doi.org/10.1051/0004-6361:20078166.

Ciarniello, M., De Sanctis, M.C., Ammannito, E., Raponi, A., Longobardo, A., Palomba, E., Carrozzo, F.G., Tosi, F., Li, J.-Y., Schröder, S.E., Zambon, F., Frigeri, A., Fonte, S., Giardino, M., Pieters, C.M., Raymond, C.A., Russell, C.T., 2017. Spectrophotometric properties of dwarf planet Ceres from the VIR spectrometer on board the Dawn mission. A&A 598, A130. 2017. https://doi.org/10.1051/0004-6361/201629490.

Chap. 1Clark, R.N., 1999. Spectroscopy of Rocks and Minerals and Principles of Spectroscopy. Chap. 1 In: Rencz, A. (Ed.), Manual of Remote Sensing. John Wiley and Sons, Inc., New York, pp. 728 pp.

Combe, J.-P., McCord, T.B., Tosi, F., Ammannito, E., Carrozzo, F.G., De Sanctis, M.C., Raponi, A., Byrne, S., Landis, M., Hughson, K.H.G., Raymond, C.A., Russell, C.T., 2016. Detection of local H_2O exposed at the surface of Ceres. Science 353 (6303). https://doi.org/10.1126/science.aaf3010.

Combe, J.-P., Singh, S., Johnson, K.E., McCord, T.B., De Sanctis, M.C., Ammannito, E., Carrozzo, F.G., Ciarniello, M., Frigeri, A., Raponi, A., Tosi, F., Zambon, F., Scully, J.E.C., Raymond, C.A., Russell, C.T., 2017. The surface composition of Ceres' Ezinu quadrangle analyzed by the Dawn mission. https://doi.org/10.1016/j.icarus.2017.12.039.

Combe, J.-P., Raponi, A., Tosi, F., De Sanctis, M.C., Carrozzo, F.G., Zambon, F., Ammannito, E., Hughson, K.H.G., Nathues, A., Hoffmann, M., Platz, T., Thangjam, G., Schorghofer, N., Schröder, S., Byrne, S., Landis, M.E., Ruesch, O., McCord, T.B., Johnson, K.E., Singh, S., Raymond, C.A., Russell, C.T., 2018. Exposed H_2O-rich areas detected on Ceres with the dawn visible and infrared mapping spectrometer. Icarus in press. https://doi.org/10.1016/j.icarus.2017.12.008.

Castillo-Rogez, J.C., McCord, T.B., 2010. Ceres' evolution and present state constrained by shape data. Icarus 205, 443–459.

Clark, R.N., 1984. Spectral properties of ice-particulate mixtures and implications for remote sensing. I – Intimate mixtures. J. Geophys. Res. 89, 6341–6348.

De Sanctis, M.C., et al., 2011. The VIR spectrometer. Space Sci. Rev. 163, 329–369.

De Sanctis, M.C., Ammannito, E., Raponi, A., Marchi, S., McCord, T.B., McSween, H.Y., Capaccioni, F., Capria, M.T., Carrozzo, F.G., Ciarniello, M., Longobardo, A., Tosi, F., Fonte, S., Formisano, M., Frigeri, A., Giardino, M., Magni, G., Palomba, E., Turrini, D., Zambon, F., Combe, J.-P., Feldman, W., Jaumann, R., McFadden, L.A., Pieters, C.M., Prettyman, T., Toplis, M., Raymond, C.A., Russell, C.T., 2015. Ammoniated phyllosilicates with a likely outer solar system origin on (1) Ceres. Nature 528 (7581), 241–244. https://doi.org/10.1038/nature16172.

De Sanctis, M.C., Raponi, A., Ammannito, E., Ciarniello, M., Toplis, M.J., McSween, H.Y., Castillo-Rogez, J.C., Ehlmann, B.L., Carrozzo, F.G., Marchi, S., Tosi, F., Zambon, F., Capaccioni, F., Capria, M.T., Fonte, S., Formisano, M., Frigeri, A., Giardino, M., Longobardo, A., Magni, G., Palomba, E., McFadden, L.A., Pieters, C.M., Jaumann, R., Schenk, P., Mugnuolo, R., Raymond, C.A., Russell, C.T., 2016. Bright carbonate deposits as evidence of aqueous alteration on (1) Ceres. Nature 536 (7614), 54–57. https://doi.org/10.1038/nature18290.

De Sanctis, M.C., Ammannito, E., McSween, H.Y., Raponi, A., Marchi, S., Capaccioni, F., Capria, M.T., Carrozzo, F.G., Ciarniello, M., Fonte, S., Formisano, M., Frigeri, A., Giardino, M., Longobardo, A., Magni, G., McFadden, L.A., Palomba, E., Pieters, C.M., Tosi, F., Zambon, F., Raymond, C.A., Russell, C.T., 2017. Localized aliphatic organic

material on the surface of Ceres. Science 355, 719–722. https://doi.org/10.1126/science.aaj2305.
Feierberg, M.A., Lebofsky, L.A., Larson, H.P., 1981. Spectroscopic evidence for aqueous alteration products on the surface of low-albedo asteroids. Geochim. Cosmochim. Acta 45, 971–981. https://doi.org/10.1016/0016-7037.
Frigeri, A., DeSanctis, M.C., Ammannito, E., Tosi, F., Ciarniello, M., Zambon, F., Carrozzo, F.G., Raponi, A., McCord, T., Raymond, C.A., Russell, C.T., 2018. The spectral parameter maps of Ceres from NASA/Dawn VIR Data. Icarus. https://doi.org/10.1016/j.icarus.2018.04.019.
Hanley, J., Dalton III, J.B., Chevrier, V.F., Jamieson, C.S., Barrows, R.S., 2014. Reflectance spectra of hydrated chlorine salts: the effect of temperature with implications for Europa. J. Geophys. Res. 119, 2370–2377.
Hapke, B., 1981. Bidirectional reflectance spectroscopy. I – Theory. J. Geophys. Res. 86, 3039–3054. https://doi.org/10.1029/JB086iB04p03039.
Hughson, K.H.G., Russell, C.T., Williams, D.A., Buczhowski, D.L., Mest, S.C., Pasckert, J.H., Scully, J.E.C., Combe, J.-P., Platz, T., Ruesch, O., Preusker, F., Jaumann, R., Nass, A., Roatsch, NathuesA., Schaefer, M., Schmidt, B.E., Chilton, H.T., Ermakov, A., Singh, S., McFadden, L.A., Raymond, C.A., 2017. The Fejokoo (Fejokoo) quadrangle of Ceres: Geologic map and geomorphological evidence for ground ice mediated surface processes. Icarus. https://doi.org/10.1016/j.icarus.2017.09.035.
International Astronomical Union, 2006. IAU General Assembly Newspaper "NVNCIO SIDEREO III". International Astronomical Union, Prague, Czech Republic 12 Aug 2006.
Jaumann, R., Stephan, K., Krohn, K., Matz, K.-D., Otto, K., Neumann, W., Kneissl, T., Schmedemann, N., Schroeder, S., Tosi, F., De Sanctis, M.C., Preusker, F., Buczkowski, D.L., Capacioni, F., Carsentry, U., Elgner, S., von der Gathen, I., Giebner, T., Hiesinger, H., Hoffmann, M., Kersten, E., Li, J.-Y., McCord, T.B., McFadden, L., Mottola, S., Nathues, A., Neesemann, A., Raymond, C.A., Roatsch, T., Russell, C.T., Schmidt, B., Schulzeck, F., Wagner, R., Williams, D.A., 2016. Age-dependent morphological and compositional variations on Ceres. In: Proceedings of the Lunar and Planetary Science Conference, XLVII, Abs. #1455.
Konopliv, A.S., Asmar, S.W., Bills, B.G., Mastrodemos, N., Park, R.S., Raymond, C.A., Smith, D.E., Zuber, M.T., 2011. The Dawn Gravity Investigation at Vesta and Ceres. Space Sci Rev 163, 461–486. https://doi.org/10.1007/s11214-011-9794-8. 2011.
King, T.V.V., Clark, R.N., Calvin, W.M., Sherman, D.M., Brown, R.H., 1992. Evidence for ammonium-bearing minerals on Ceres. Science 255, 1551–1553.
Lebofsky, L.A., Feierberg, MA, Tokunaga, A.T., Larson, H.P, Johnson, J.R., 1981. The 1.7-4.2-μm spectrum of asteroid 1 Ceres: Evidence for structural water in clay minerals. Icarus 48, 453–459. https://doi.org/10.1016/0019-1035.
Li, J.-Y., Nathues, A., Mottola, S., De Sanctis, M.C., Mastrodemos, N., Sykes, M.V., Russell, C.T., Raymond, C.A., Hoffmann, M., Longobardo, A., Ciarniello, M., 2015. The Phase function of Ceres at High Phase Angles. In: 46th Lunar and Planetary Conference, held March 16-20, 2015 at The Woodlands, pp. 2565 TX LPI Contribution No. 1832.
Longobardo, A., Palomba, E., Carrozzo, F.G., Galiano, A., De Sanctis, M.C., Stephan, K., Tosi, F., Raponi, A., Ciarniello, M., Zambon, F., Frigeri, A., Ammannito, E., Raymond, C.A., Russell, C.T., 2018. Mineralogy of the Occator Quadrangle. Icarus. https://doi.org/10.1016/j.icarus.2017.09.022.
McCord, ThomasB., Zambon, Francesca, 2018. The surface composition of Ceres from the Dawn mission. Icarus. https://doi.org/10.1016/j.icarus.2018.03.004.
McCord, T.B., Teeter, G., Hansen, G.B., Sieger, M.T., Orlando, T.M., 2002. Brines exposed to Europa surface conditions. J. Geophys. Res. 107, 1–5.
McCord, T.B., Sotin, C., 2005. Ceres: evolution and current state. J. Geophys. Res. 110, E5.
Milliken, R.E., Rivkin, A.S., 2009. Brucite and carbonate assemblages from altered olivine-rich materials on Ceres. Nat. Geosci. 2, 258–261.
Park, R.S., Konopliv, A.S., Bills, B.G., Rambaux, N., Castillo-Rogez, J.C., Raymond, C.A., Vaughan, A.T., Ermakov, A.I., Zuber, M.T., Fu, R.R., Toplis, M.J., Russell, C.T., Nathues, A., Preusker, F., 2016. A partially differentiated interior for (1) Ceres deduced from its gravity field and shape. Nature 537, 515–517. https://doi.org/10.1038/nature18955.
Pieters, C.M., Tompkins, S., 1999. Tsiolkovsky crater: a window into crustal processes on the lunar farside. J. Geophys. Res. 104, 21935–21950. https://doi.org/10.1029/1998JE001010.
Pieters, C.M., et al., 2017. Geologic constraints on the origin of red organic-rich material on Ceres. Meteorit. Planet. Sci. https://doi.org/10.1111/maps.13008.
Prettyman, T.H., Feldman, W.C., McSween, H.Y., Dingler, R.D., Enemark, D.C., Patrick, D.E., Storms, S.A., Hendricks, J.S., Morgenthaler, J.P., Pitman, K.M., Reedy, R.C., 2011. Dawn's Gamma Ray and Neutron Detector. Space Science Reviews 163, 371–459. https://doi.org/10.1007/s11214-011-9862-0.
Prettyman, T.H., Yamashita, N., Castillo-Rogez, J.C., Feldman, W.C., Lawrence, D.J., McSween, H.Y., Schorghofer, N., Toplis, M.J., Forni, O., Joy, S.P., Marchi, S., Platz, T., Polanskey, C.A., De Sanctis, M.C., Rayman, M.D., Raymond, C.A., Russell, C.T., 2017. Extensive water ice within Ceres' aqueously altered regolith: evidence from nuclear spectroscopy. Science 35, 55–59.
Palomba, E., Longobardo, A., De Sanctis, M.C., Stein, N.T., Ehlmann, B., Galiano, A., Raponi, A., Ciarniello, M., Ammannito, E., Cloutis, E., Carrozzo, F.G., Capria, M.T., Stephan, K., Zambon, F., Tosi, F., Raymond, C.A., Russell, C.T., 2017. Compositional differences among Bright Spots on Ceres. Icarus. https://doi.org/10.1016/j.icarus.2017.09.020.
Preusker, F., Scholten, F., Matz, K.-D., Elgner, S., Jaumann, R., Roatsch, T., Joy, S.P., Polanskey, C.A., Raymond, C.A., Russell, C.T., 2016. Dawn at Ceres — Shape Model and Rotational State. Lunar and Planetary Science Conference 47, 1954.
Raponi, A., Carrozzo, F.G., Zambon, F., De Sanctis, M.C., Ciarniello, M., Frigeria, A., Ammannito, E., Tosi, F., Combe, J.-Ph., Longobardo, A., Palomba, E., Pieters, C.M., Raymond, C.A., Russell, C.T., 2017. Mineralogical mapping of Coniraya quadrangle of the dwarf planet Ceres. https://doi.org/10.1016/j.icarus.2017.10.023.
Raponi, A., De Sanctis, M.C., Frigeri, A., Ammannito, E., Ciarniello, M., Formisano, M., Combe, J.-Ph., Magni, G., Tosi, F., Carrozzo, F.G., Fonte, S., Giardino, M., Joy, S.P., Polanskey, C.A., Rayman, M.D., Capaccioni, F., Capria, M.T., Longobardo, A., Palomba, E., Zambon, F., Raymond, C.A., Russell, C.T., 2018. Variations in the amount of water ice on Ceres' surface suggest a seasonal water cycle. Sci. Adv. 4, eaao3757.
Rivkin, A.S., Volquardsen, E.L., Clark, B.E., 2006. The surface composition of Ceres: discovery of carbonates and iron-rich clays. Icarus 185, 563–567.
Roatsch, T., Kersten, E., Matz, K.-D., Preusker, F., Scholten, F., Jaumann, R., Raymond, C.A., Russell, C.T., 2016. High-resolution Ceres high altitude mapping orbit atlas derived from dawn framing camera images. Planet. Space Sci. 129, 103–107.
Roatsch, Th., Kersten, E., Matz, K.-D., Preusker, F., Scholten, F., Jaumann, R., Raymond, C.A., Russell, C.T., 2017. High-resolution Ceres low altitude mapping orbit atlas derived from dawn framing camera images. PSS 140, 74–79.
Ruesch, O., Platz, T., Schenk, P., McFadden, L.A., Castillo-Rogez, J.C., Quick, L.C., Byrne, S., Preusker, F., O'Brien, D.P., Schmedemann, N., Williams, D.A., Li, J.-Y., Bland, M.T., Hiesinger, H., Kneissl, T., Neesemann, A., Schaefer, M., Pasckert, J.H., Schmidt, B.E., Buczkowski, D.L., Sykes, M.V., Nathues, A., Roatsch, T., Hoffmann, M., Raymond, C.A., Russell, C.T., 2016. Cryovolcanism on Ceres. Science 353 (6303), aaf4286. https://doi.org/10.1126/science.aaf4286.
Russell, C.T., Raymond, C.A., Ammannito, E., Buczkowski, D.L., De Sanctis, M.C., Hiesinger, H., Jaumann, R., Konopliv, A.S., McSween, H.Y., Nathues, A., Park, R.S., Pieters, C.M., Prettyman, T.H., McCord, T.B., McFadden, L.A., Mottola, S., Zuber, M.T., Joy, S.P., Polanskey, C., Rayman, M.D., Castillo-Rogez, J.C., Chi, P.J., Combe, J.P., Ermakov, A., Fu, R.R., Hoffmann, M., Jia, Y.D., King, S.D., Lawrence, D.J., Li, J.-Y., Marchi, S., Preusker, F., Roatsch, T., Ruesch, O., Schenk, P., Villarreal, M.N., Yamashita, N., 2016. Dawn arrives at Ceres: Exploration of a small, volatile-rich world. Science 353 (6303), 1008–1010.
Schenk, P.M., 1989. Crater formation and modification on the icy satellites of Uranus and Saturn: Depth/diameter and central peak occurence. J. Geophys. Res. 94, 3813–3832. https://doi.org/10.1029/JB094iB04p03813.
Schröder, S.E., Mottola, S., Carsenty, U., Ciarniello, M., Jaumann, R., Li, J.-Y., Longobardo, A., Palmer, E., Pieters, C., Preusker, F., Raymond, C.A., Russell, C.T., 2017. Resolved spectrophotometric properties of the Ceres surface from dawn framing camera images. Astrophys. Earth Planet. Astrophys. https://doi.org/10.1016/j.icarus.2017.01.026.
Sierks, H., Keller, H.U., Jaumann, R., Michalik, H., Behnke, T., Bubenhagen, F., Büttner, I., Carsenty, U., Chirstensen, R., Enge, R., Fiethe, B., Gutiérrez Marqués, P., Hartwig, H., Krüger, KühneW., 2011. The Dawn Framing Camera. Space Science Reviews 163, 263–327. https://doi.org/10.1007/s11214-011-9745-4.
Stein, N., et al., 2017. The formation and evolution of bright spots on Ceres. Icarus. https://doi.org/10.1016/j.icarus.2017.10.014.
Tosi, F., Carrozzo, F.G., Zambon, F., Ciarniello, M., Frigeri, A., Combe, J.-P., De Sanctis, M.C., Hoffmann, M., Longobardo, A., Nathues, A., Raponi, A., Thangjam, G., Ammannito, E., Krohn, K., McFadden, L.A., Palomba, E., Pieters, C.M., Stephan, K., Raymond, C.A., Russell, C.T., 2018. Mineralogical analysis of the Ac-H-6 Haulani quadrangle of the dwarf planet Ceres. Icarus. https://doi.org/10.1016/j.icarus.2017.08.012.
Zambon, F., Raponi, A., Tosi, F., De Sanctis, M.C., McFadden, L.A., Carrozzo, F.G., Longobardo, A., Ciarniello, M., Krohn, K., Stephan, K., Palomba, E., Pieters, C.M., Ammannito, E., Russell, C.T., Raymond, C.A., 2017. Spectral analysis of Ahuna Mons from dawn mission's visible-infrared spectrometer. Geophys. Res. Lett. 44, 97–104. https://doi.org/10.1002/2016GL071303.